Accepted by The Astronomical Journal
Preprint typeset using LaTeX style emulateapj v. 12/14/05

arXiv:astro-ph/0608294v1 14 Aug 2006

VIRGO CLUSTER EARLY-TYPE DWARF GALAXIES WITH THE SLOAN DIGITAL SKY SURVEY. II. EARLY-TYPE DWARFS WITH CENTRAL STAR FORMATION

Thorsten Lisker, Katharina Glatt, Pieter Westera, and Eva K. Grebel
Astronomical Institute, Dept. of Physics and Astronomy, University of Basel, Venusstrasse 7, CH-4102 Binningen, Switzerland

Accepted by The Astronomical Journal

ABSTRACT

Despite the common picture of an early-type dwarf (dE) as a quiescent galaxy with no star formation and little gas, we identify 23 dEs that have blue central colors caused by recent or ongoing star formation in our sample of 476 Virgo cluster dEs. In addition, 14 objects that were mostly classified as (candidate) BCDs have similar properties. Among the certain cluster members, the dEs with blue centers reach a fraction of more than 15% of the dE population at brighter ($m_\mathrm{B} \leq 16$) magnitudes. A spectral analysis of the centers of 16 galaxies reveals in all cases an underlying old population that dominates the mass, with $M_\mathrm{old} \geq 90\%$ for all but one object. Therefore the majority of these galaxies will appear like ordinary dEs within $\sim$ one Gigayear or less after the last episode of star formation. Their overall gas content is less than that of dwarf irregular galaxies, but higher than that of ordinary dEs. Their flattening distribution suggests the shape of a thick disk, similar to what has been found for dEs with disk features in Paper I of this series. Their projected spatial distribution shows no central clustering, and their distribution with projected local density follows that of irregular galaxies, indicative of an unrelaxed population. This is corroborated by their velocity distribution, which displays two side peaks characteristic of recent infall. We discuss possible formation mechanisms (ram-pressure stripping, tidally induced star formation, harassment) that might be able to explain both the disk shape and the central star formation of the dEs with blue centers.

Subject headings: galaxies: dwarf — galaxies: structure — galaxies: evolution — galaxies: stellar content — galaxies: clusters: individual (Virgo) — galaxies: fundamental parameters

1. INTRODUCTION

Early-type dwarf galaxies are the most numerous type of galaxy in clusters, suggesting that the vigorous forces acting within a cluster environment might actually be creating them. At least theoretically, this could come about via a morphological transformation of infalling galaxies, like e.g. ram-pressure stripping of irregular galaxies (Gunn & Gott 1972), or so-called harassment of late-type spirals (Moore et al. 1996). While these scenarios would in principle also be able to explain the famous morphology-density relation (e.g. Dressler 1980), unambiguous observational proofs are difficult to obtain. Early-type dwarfs are characterized by their smooth, regular appearance, while any possible progenitor galaxy probably displays a different overall structure, before a morphological transformation occurs. Moreover, early-type dwarfs themselves are not a homogeneous class of objects. In addition to the classical dwarf ellipticals, Sandage & Binggeli (1984) introduced the class of dwarf S0 (dS0) galaxies, which were conjectured to have disk components, based on indications like high flattening or a bulge-disk-like profile (Binggeli & Cameron 1991). Following up on the discovery of spiral structure in an early-type dwarf (Jerjen et al. 2000) and on similar other discoveries, we identified 41 Virgo cluster early-type dwarfs with disk features in Lisker et al. (2006, hereafter Paper I), and argued that they constitute a population of disk-shaped objects. Furthermore, nucleated and non-nucleated dwarf ellipticals show significantly different clustering properties (Binggeli et al. 1987) and flattening distributions (Ryden & Terndrup 1994; Binggeli & Popescu 1995).

Aside from this structural heterogeneity, color differences have been reported as well (Rakos & Schombert 2004; Lisker et al. 2005), hinting at a range of stellar populations in early-type dwarfs. While the classical dwarf ellipticals are typically considered not to have recent or ongoing star formation and no significant gas or dust content (e.g. Grebel 2001; Conselice et al. 2003), the well known Local Group galaxy NGC 205 constitutes a prominent example for an early-type dwarf that does exhibit central star formation, gas, and dust (Hodge 1973). More examples are NGC 185 (Hodge 1963) and the apparently isolated galaxy IC 225 (Gu et al. 2006). Furthermore, Conselice et al. (2003) report a 15% HI detection rate for early-type dwarfs in the Virgo cluster. All these objects are morphologically early-type dwarfs, but form a heterogeneous family of objects, which we assign the common abbreviation “dE”, thereby including galaxies classified as dwarf elliptical or as dS0.

Based on the general idea of gas removal due to effects like ram-pressure stripping, numerous observational studies have focused on comparing the properties of gas-rich dwarf irregular (dIrr) galaxies and gas-poor dEs and dwarf spheroidals (dSphs), attempting to confirm or reject a possible evolutionary relation between them. Thuan (1985) found in his study of optical–near-infrared colors the metallicity ranges of dIrrs and Virgo dEs to be “mutually exclusive”. In their spectroscopic analysis of oxygen abundances of planetary nebulae in Local Group dEs and dSphs, Richer et al. (1998) also found a significant offset to the respective abundances of dIrrs.

Electronic address: tlisker@astro.unibas.ch

Similarly, Grebel et al. (2003) recently showed for the Local Group that this metallicity difference exists even when considering only the respective old stellar populations of dIrrs and dSphs, indicative of more intense star formation and enrichment in dSphs. Thuan (1985) and Binggeli (1985) also noted that many Virgo dEs are nucleated, while none of the dIrrs are. Bothun et al. (1986) concluded that Virgo dIrrs would have to fade by ∼1.5 mag in B to fall into the optical–near-infrared color range of dEs. However, the bulk of faded dIrrs would then have an effective surface brightness $\mu_{\rm B,e} > 25$mag/arcsec^2, substantially lower than the observed values of dEs.

Despite these counter-arguments, potential dIrr/dE "transition types" have frequently been discussed (e.g. Ferguson & Binggeli 1994; Johnson et al. 1997; Knezek et al. 1999). Recently, van Zee et al. (2004) pointed out the "remarkable commonality" between dEs and dIrrs with respect to their surface brightness distributions and metallicity-luminosity relations. These authors found significant rotation in several bright dEs, upon which they base their discussion about the possibility that these very dEs may have formed via ram-pressure stripping of dIrrs. While van Zee et al. (2004) admitted that dEs (in Virgo) might actually form through various processes, they argued that every dE must have been gas-rich and star-forming in the past, and would thus inevitably have been classified as dIrr. However, these properties also apply to blue compact dwarf (BCD) galaxies, which have often been discussed in the literature as potential dE progenitors.

An important difference between dIrrs and BCDs was highlighted by Bothun et al. (1986), who characterized dIrrs as an "odd combination of rather blue colors, yet quite low surface brightness," indicative of a low surface mass density. In contrast, BCDs have a much higher surface brightness, suggesting a higher surface mass density, since they are not bluer than the dIrrs. Whether or not BCDs could indeed be the gas-rich, star-forming progenitors of dEs has been discussed controversially (e.g. Bothun et al. 1986; Drinkwater et al. 1996; Guzman et al. 1996; Papaderos et al. 1996). A glance at the color images[1] of Virgo cluster galaxies that were classified as (candidate) BCDs reveals what might be one reason for this controversy: these objects do not constitute a homogeneous class, but they vary strongly in size, (ir)regularity, and the fraction of area dominated by blue light with respect to the total area of the galaxy. It might thus be more promising to simply look for plausible dE progenitors among the BCDs, instead of attempting to draw conclusions about this class as a whole.

Interestingly, Bothun et al. (1986) mentioned that the BCDs in their sample look similar to NGC 205. Could dEs with central star formation thus bridge the evolutionary gap from quiescent dEs to potentially starbursting progenitors? To our knowledge, Vigroux et al. (1984) were the first to identify a central star formation region in a dwarf elliptical outside the Local Group. Recently, Gu et al. (2006) presented a similar dE with ongoing star formation in its center. In Paper I of this series (Lisker et al. 2006), we identified nine Virgo early-type dwarfs with central irregularities likely to be caused by dust or gas, and found that all of them have a blue center. In the present paper (Paper II), we follow up on these objects, and systematically search the Virgo cluster for such dEs with blue centers. This is made possible by the publicly available data of the Sloan Digital Sky Survey (SDSS) Data Release 4 (DR4, Adelman-McCarthy et al. 2006) which covers almost the whole Virgo cluster with multiband optical imaging and partly with spectroscopy. Our data and sample are described in Sects. 2 and 3, respectively. Results from image analysis are presented in Sect. 4, followed by the spectral analysis in Sect. 5. Section 6 focuses on the gas content of our galaxies. The systematic properties of dEs with blue centers are given in Sect. 7. Their evolutionary role is discussed in Sect. 8, followed by a summary and outlook in Sect. 9.

2. DATA

2.1. *SDSS imaging*

The SDSS DR4 covers all galaxies listed in the Virgo Cluster Catalog (VCC, Binggeli et al. 1985) with a declination of $\delta \lesssim 16.^\circ25$, except for an approximately $2^\circ \times 2.^\circ5$ area at $\alpha \approx 186.^\circ2$, $\delta \approx +5.^\circ0$. It provides reduced and calibrated images taken in the u, g, r, i, and z bands with an effective exposure time of 54s in each band (see also Stoughton et al. 2002). The pixel scale of $0.''396$ corresponds to a physical size of 30pc when adopting a Virgo cluster distance of $d = 15.85$Mpc, i.e. a distance modulus $m - M = 31.0$ mag (see e.g. Ferrarese et al. 2000), which we use throughout. The SDSS imaging camera (Gunn et al. 1998) takes data in drift-scanning mode nearly simultaneously in the five photometric bands, and thus combines very homogeneous multicolor photometry with large area coverage, good resolution, and sufficient depth to enable a systematic analysis of early-type dwarfs. The images have an absolute astrometric accuracy of RMS $\leq 0.''1$ per coordinate, and a relative accuracy between the r band and each of the other bands of less than 0.1 pixels (Pier et al. 2003). They can thus easily be aligned using their astrometric calibration and need not be registered manually. The RMS of the noise per pixel corresponds to a surface brightness of approximately 24.2mag/arcsec^2 in the u-band, 24.7 in g, 24.4 in r, 23.9 in i, and 22.4 in z. The typical total signal-to-noise ratio (S/N) of a bright dE ($m_{\rm B} \approx 14$) amounts to about 1000 in the r-band within an aperture radius of approximately two half-light radii. For a faint dE ($m_{\rm B} \approx 18$) this value is typically about 50. While the S/N in the g and i-band is similar to the above value, it is several times lower in the z-band and more than ten times lower in the u-band. Therefore u and z will not be used in the following analysis.

The SDSS provides photometric measurements for our galaxies, but we found these to be incorrect in many cases (Lisker et al. 2005). The SDSS photometric pipeline significantly overestimates the local sky flux around the Virgo dEs due to their large apparent sizes and low surface brightness outskirts. This affects the measurement of isophotal and Petrosian radii, the profile fits, and subsequently the calculation of total magnitudes, which can be wrong by up to 0.5 mag. Therefore, we use B magnitudes from the VCC throughout the paper, and defer calculation of total magnitudes from SDSS data to a more detailed photometric study of the Virgo dEs.

---

[1] Using the Sloan Digital Sky Survey Image List Tool, http://cas.sdss.org/astro/en/tools/chart/list.asp, Authors: J. Gray, A. Szalay, M. Nieto-Santisteban, and T. Budavari

2.2. *SDSS spectroscopy*

The centers of several galaxies are also covered by the SDSS spectroscopic survey, which provides fiber spectra with a wavelength coverage of $3800-9200$ Å and a resolution of 1800 or larger. The spectra are binned in logarithmic wavelength, such that the wavelength interval of one pixel along the dispersion axis corresponds to a constant velocity interval of 69 km s^{-1} (York et al. 2000). The fiber diameter corresponds to an angular size of $3''$, which translates into 231pc at a distance $d = 15.85$Mpc. Typical half-light radii of the brighter dEs range from $\sim 10''$ to $\sim 25''$ (Binggeli & Cameron 1991), or from 0.8 to 1.9 kpc. *Therefore, spectral information is only available for the very central region of the dEs.*

2.3. *Radial velocities*

Heliocentric velocities are available for 198 dEs of our sample of 414 dEs from Paper I that are listed as certain Virgo cluster members in Binggeli et al. (1985) and Binggeli et al. (1993). Velocities were taken from the NASA/IPAC Extragalactic Database (NED), originally provided by the SDSS and by the following studies: Binggeli et al. (1985); de Vaucouleurs et al. (1991); Strauss et al. (1992); Binggeli et al. (1993); Young & Currie (1995); Drinkwater et al. (1996); Grogin et al. (1998); Falco et al. (1999); Gavazzi et al. (2000); van Driel et al. (2000); Conselice et al. (2001); Simien & Prugniel (2002); Caldwell et al. (2003); Geha et al. (2003); Gavazzi et al. (2004).

Four of these galaxies, however, have velocities above 6000 km s^{-1} from recent data (SDSS and Conselice et al. 2001). Since the velocities of known Virgo cluster members are lower by more than a factor of two, we change the membership status of these galaxies (VCC 0401, VCC 0838, VCC 1111, VCC 1517) to “possible member”. This leaves us with a subsample of 194 dEs that are certain cluster members and for which radial velocity measurements are available.

3. SAMPLE

3.1. *Sample selection*

In Paper I of this series, we put together a sample of Virgo cluster dEs that comprises all dEs with $m_{\mathrm{B}} \leq 18.0$ mag that are listed in the VCC, that are covered by the SDSS, and that are certain or possible cluster members according to Binggeli et al. (1985) and Binggeli et al. (1993). While objects with uncertainties were initially included, we then excluded all galaxies that appeared to be possible dwarf irregulars due to asymmetric shapes. Objects classified as “dE/dIrr” were not included. 25 galaxies classified as (candidate) dE in the VCC are not covered by the SDSS DR4. The resulting sample comprises 476 early-type dwarfs, 410 of which are certain cluster members (see Sect. 2.3). Note that our magnitude limit of $m_{\mathrm{B}} \leq 18.0$ mag corresponds to the magnitude up to which the VCC was found to be complete (Binggeli et al. 1985). With a distance modulus of $m - M = 31.0$ mag, this translates into $M_{\mathrm{B}} \leq -13.0$ mag.

In this sample, we identified several dEs with irregular or clumpy central features likely caused by gas and dust (cf. Fig. 6 of Paper I). By dividing the background-subtracted aligned g and i-band images provided by Paper I, we obtain color maps that are not calibrated, yet are useful to look for significant color gradients. Most of the objects just described have a central region whose color is clearly bluer than that of the rest of the galaxy, similar to the dE recently presented by Gu et al. (2006). Using these color maps, we visually searched all 476 early-type dwarf galaxies that were presented in Paper I for such a blue center. As a complementary check we then examined the radial $g-i$ color profiles (Sect. 4.1) of the thus selected galaxies to confirm the presence of a clear color gradient.

23 out of 476 dEs (16/410 certain cluster members) entered our working sample of galaxies with blue centers (Figs. 1, 2, and 3). We shall term these objects “dE(bc)s” hereafter. Note that the presence of *weak* color gradients (either negative or positive) in dEs has been reported in the literature (e.g. Gavazzi et al. 2005). Such objects are not the focus of this study; we rather aim at dEs with a blue center, i.e. a significant positive gradient. The distinction between a weak and a significant gradient might appear somewhat arbitrary; however, a detailed and quantitative study of color gradients of our full dE sample is beyond the scope of this paper and will be presented elsewhere. The weakest gradient visually selected by us is that of VCC 0308, with a color difference of 0.1 mag between inner and outer regions (see Fig. 2).

We point out that the dE(bc)s were morphologically classified as dwarf ellipticals or dS0s by Sandage & Binggeli (1984), and were confirmed as early-type dwarfs in our Paper I. While Ferrarese et al. (2006) suggest to reclassify four dE(bc)s as dE/dIrr based on their blue central colors and irregular isophotal shapes in the center, we do not use color as a criterion for *morphological* classification. The *central* irregularities are the reason for which they were assigned to the class dS0 (Binggeli & Cameron 1991), but their overall appearance is smooth and regular, as can be seen from the combined images (Figs. 1 to 3). Complementary to these, we show isophotal contours of the dE(bc)s in Fig. 4 (see Sect. 4.1). There, the central irregularities in several dE(bc)s can be seen, which are also revealed by the unsharp mask images. Outside of the central region, though, the isophotes are regularly shaped, confirming the early-type dwarf morphology of these galaxies.

Our preselection of dEs relies on the classification given in the VCC, and on the subsequent examination of the combined images in Paper I. However, the intial selection was based on photographic plates, which are most sensitive to the blue light. Therefore, if the color distribution of a candidate dE(bc) would be quite asymmetric or if the blue central region would make up for a rather large fraction of the total light, this galaxy might not have been classified as dE in the first place.[2] We thus decided to use the color-combined images provided by the SDSS Image List Tool[3] to search all objects classified as irregular galaxy or as blue compact dwarf (BCD; including candidates) for galaxies that look similar to the dE(bc)s, i.e., that have a regular outer shape and a color similar to the dEs, while having a blue inner region. We found 12 such objects (10 certain cluster members). Furthermore, two galaxies classified as E/S0 with magnitudes similar to the brighter dEs show the same appearance; both are certain cluster members. Images and color profiles of these additional galaxies are presented in Figs. 5 and 6, and their isophotal contours are shown in Fig. 7.

---

[2] Note that the dE(bc)s identified above were classified as dE *despite* their having been observed in blue light, in which the light of young stars – if present – dominates.

[3] http://cas.sdss.org/astro/en/tools/chart/list.asp, Authors: J. Gray, A. Szalay, M. Nieto-Santisteban, and T. Budavari

To ensure that we are not mixing different types of galaxies, we shall use separate samples of objects in the course of our study: the *main sample* comprising the 23 galaxies classified as dE that have a blue center, and an *additional sample* comprising the 14 galaxies classified other than dE that are similar in appearance to the dE(bc)s. Table 1 lists our selected objects along with their classification.

3.2. *Presence of disks*

In Paper I we presented a systematic search for disk features in Virgo cluster dEs, which we detected in 41 out of 476 objects (including candidates). We showed that these galaxies – termed dE(di)s – are not simply dwarf ellipticals that just have an embedded disk component, but appear to be instead a population of genuine disk galaxies, i.e. flat oblate objects. Amongst the 23 dE(bc)s of our main sample, five are (candidate) dE(di)s, or 4 out of 16 if only certain cluster members are counted. The fraction of dE(di)s among the full dE sample is roughly about 25% at the median B magnitude of the dE(bc)s (14.86, again counting only certain cluster members). In a randomly chosen sample of 16 dEs we would thus expect to find 4 dE(di)s, which equals our observed number. Two galaxies in the additional sample also show possible disk features (VCC 0135: possibly spiral arms, VCC 1437: possibly spiral arms and a bar). Both are certain cluster members, so the number of 2 out of 10 objects with disks is again consistent with the above fractions. A detailed comparison of the properties of dE(bc)s, dE(di)s, and ordinary dEs is presented in Sect. 7.

4. IMAGE ANALYSIS

4.1. *Techniques*

The study presented in Paper I provides us with background-subtracted, aligned g, r, and i-band images, a combined image, unsharp masks, and an elliptical aperture for each object. A detailed description can be found in Paper I. Briefly, combined images were obtained by co-adding the g, r, and i-band images to increase the S/N. From these we produced unsharp masks with various kernel sizes (using *IRAF*[4]*/gauss*; Tody 1993), as well as isophotal contour diagrams (using *IRAF/newcont*). An elliptical aperture for each galaxy was determined by performing ellipse fits with *IRAF/ellipse* on the combined image, and then choosing by eye one of the outer elliptical isophotes to trace best the outer shape of the galaxy. This isophote was usually between 1 and 2 half-light radii.

The SDSS flux calibration was applied to the aligned g and i-band images for each source, following the instructions on the SDSS webpage[5]. These images were then divided by each other, converted into magnitudes, and corrected for Galactic extinction (Schlegel et al. 1998), yielding proper $g - i$ color maps. From the same images we obtained radial intensity profiles by azimuthally averaging over elliptical annuli with *IRAF/ellipse*. We used geometric steps (i.e., steps that increase by a constant factor) and a fixed position angle, ellipticity, center, and semi-major axis. The ratio of the g and i-band fluxes was then converted into magnitudes, yielding radial $g-i$ color profiles, where radius is calculated from semi-major (a) and semi-minor axis (b) as $\sqrt{ab}$. Disturbing foreground stars and background galaxies were masked prior to profile calculation.

4.2. *Results from the image analysis*

In Figs. 1 to 6 we present for each galaxy the radial color profile, the combined image, the unsharp mask created with a Gaussian filter with $\sigma = 4$ pixels, and the color map. The color profiles contain two types of errors: the black error bars give the uncertainty calculated from the S/N only, whereas the grey error bars represent the *azimuthal* variation of the color at the respective radius (which, of course, includes S/N-effects). A color distribution that is not symmetric with respect to the galaxy center (e.g. in VCC 1617, see Fig. 2) or is somewhat irregular (e.g. in VCC 0170, see Fig. 1) leads to an azimuthal variation of color significantly larger than the uncertainty from S/N only.

In many cases the unsharp masks reveal central irregularities likely caused by gas and dust features or by asymmetric star forming regions. On average, the central irregularities are stronger and the blue central regions are larger for galaxies of the additional sample as compared to those of main sample.

Obviously, some galaxies have a relatively constant outer color and abruptly start to become bluer when going inwards (e.g. VCC 0173), while others display a gradual color change from the outer regions to the center (e.g. VCC 1501). Although it is not always unambiguous which of the two cases applies to an object, we attempted to sort the dE(bc)s in Figs. 1 to 3, as well as the (candidate) BCDs of the additional sample in Figs. 5 and 6, according to the color profile shape: starting with those that have a constant outer color until a steep gradient sets in abruptly, to those with a smooth gradient. We found no correlations of this profile shape with either magnitude, radius, or surface brightness.

In order to compare the $g-i$ colors of the dE(bc)s with those of "ordinary" dEs, we make use of the colors computed by Lisker et al. (2005) for 228 galaxies of our full dE sample, excluding dE(bc)s. Those colors were derived from aperture photometry on the SDSS images, using circular apertures with a radius equalling the half-light radius. We performed a linear fit to the color-magnitude relation of B magnitude versus $g - i$ color, yielding an average dE color for each magnitude with a standard deviation of 0.06 mag. These values are shown in Figs. 1 to 6 for each galaxy: the grey shaded bands enclose the 2-σ range of color at each galaxy's magnitude. For most galaxies, the outer color is still bluer than the typical dE color; for several objects it is even bluer than the 2-σ range. Note that the above fit has been performed on dE colors computed *within* the half-light radius; however, no strong gradient is to be expected since all dE(bc)s have been excluded from the fit. Thus, the relatively blue outer colors of the dE(bc)s could hint at a younger age of the dE(bc)s as a whole, a lower metallicity, or a shorter time since the last star formation activity in the outer regions as compared to ordinary dEs. A spectroscopic examination of the stellar content of the dE(bc)s is possible at least for the centers of several galaxies, as presented in the following section.

---

[4] IRAF is distributed by the National Optical Astronomy Observatories, which are operated by the Association of Universities for Research in Astronomy, Inc., under cooperative agreement with the National Science Foundation.

[5] http://www.sdss.org/dr4/algorithms/fluxcal.html

5. SPECTRAL ANALYSIS

In order to explore the stellar content of our objects, we examine integrated spectra from the SDSS DR4 as described in Sect. 2.2. These are taken with fibers of a diameter of 3″, corresponding to a physical size of 231 pc at a distance $d = 15.85$Mpc. 10 such spectra are available for the main dE(bc) sample, one of which (VCC 0046) proved too noisy for a stellar population analysis. Seven spectra are available for the additional sample. These 16 galaxies are labelled in the last column of Table 1 with "S". Six dE(bc)s of the main sample and six galaxies of the additional sample display Balmer line emission (see Table 1). One more dE(bc) of the main sample and three galaxies of the additional sample are detected in the Hα imaging study of Boselli et al. (2002). This is a clear indication for ongoing star formation in the dE(bc)s. We note that the overall emission line strengths are larger for objects of the additional sample than for those of the main sample.

We determine the stellar content using a population synthesis method, described in Cuisinier et al. (2006), wherein the spectra are fitted to synthetic composite stellar populations' spectra. Similar methods have already been employed by Cid Fernandes et al. (2003), Kong et al. (2003), Westera et al. (2004), and Gu et al. (2006); the latter describe a dE with blue center very similar to our objects.

5.1. *Synthetic stellar populations*

The synthetic composite stellar populations were composed using simple stellar population (SSP) spectra from three different libraries of SSPs. The first SSP library (hereafter the "BC99" library) was produced using the Bruzual and Charlot 2000 Galaxy Isochrone Spectral Synthesis Evolution Library (GISSEL) code (Charlot & Bruzual 1991; Bruzual & Charlot 1993, 2000), implementing the Padova 2000 isochrones (Girardi et al. 2000) combined with the BaSeL 3.1 "Padova 2000" stellar library (Westera et al. 2002; Westera 2001). The second SSP library, "Starburst", consists of spectra from the STARBURST99 data package (Leitherer et al. 1999) including nebular continuum emission (Fig. 1 on the STARBURST99 web site, http://www.stsci.edu/science/starburst99/). It implements the BaSeL 2.2 library (Lejeune et al. 1997, 1998), and for stars with strong mass loss it also takes into account extended model atmospheres by Schmutz et al. (1992), combined with the Geneva isochrones (Meynet et al. 1994; Schaller et al. 1992; Schaerer et al. 1993a,b; Charbonnel et al. 1993). For old populations, the "BC99" spectrum was used, since the Starburst99 data package only contains spectra up to 900 Myr. Additionally to these two libraries, we also used a library with higher spectral resolution, "BC03", produced by employing the 2003 version of the GISSEL code (Bruzual & Charlot 2003) and the Padova 1995 isochrones (Fagotto et al. 1994; Girardi et al. 1996) combined with the STELIB (Le Borgne et al. 2003) stellar library. The nebular continuum emission was also added to the spectra in the "BC99" and "BC03" libraries, in the same way as described by Leitherer et al. (1999).

5.2. *Fit to model spectra: procedure*

The spectra cover a wavelength range of around 3820 Å to 9200 Å, but the wavelength region above 8570 Å is too much affected by telluric lines, so we fit the full spectra from 3820 Å to 8570 Å, except for those various parts of the spectra showing "contamination" from different emission and/or telluric line sources. Table 2 lists all the regions that were omitted.

We corrected the spectra for redshift and for Galactic foreground extinction using the values from Schlegel et al. (1998) and the extinction law of Fluks et al. (1994). In the eight cases with Hα and Hβ emission we also corrected for internal gas extinction, again using the Fluks et al. extinction law. The extinction constants $E(B-V) = A_V/3.266$ were estimated from the $H\alpha/H\beta$ Balmer decrements following Torres-Peimbert et al. (1989), adopting intrinsic ratios of the emission line fluxes $I_{H\alpha}/I_{H\beta} = 2.87$ (Osterbrock 1989). In order to properly determine the emission line strengths, we first had to remove the contribution from the absorption lines of the underlying stellar populations. This was done by making a first fit to the spectra employing the method described in the following paragraph, using the highest resolution library ("BC03", see above), and then subtracting the best fit spectra from the observed spectra as illustrated in Fig. 8. The so found values for $E(B-V)$ were multiplied by a factor of 0.44 to correct for systematic differential extinction between the stellar populations and the gas (Calzetti et al. 2000). In the cases where the spectrum displays only Hα but no Hβ emission, we assume the internal extinction to be negligible: in all of these spectra the emission is much weaker than in the cases with both Hα and Hβ emission, in which the lowest value for $E(B-V)$ is already close to zero ($E(B-V) = 0.02$). The average value for internal extinction of the eight galaxies with Hα and Hβ emission is $E(B-V) = 0.10$. Note that the problem of apparent truncation of strong emission lines in SDSS spectra reported by Kniazev et al. (2004) does not occur in any of our spectra.

We modelled the actual population as being composed of an old (≥ 1 Gyr), an intermediate-age (10 Myr to 1 Gyr), and a young (< 10 Myr) stellar population. While there is no standard definition for this age terminology, these age ranges are chosen to reflect the significant changes in the spectrum of an SSP with increasing age. Similar values were used e.g. by Cid Fernandes et al. (2003); Maraston (2005); Gu et al. (2006). The characteristics and free parameters of the three populations are summarized in Table 3. In order to confine the parameter space to as few dimensions as possible and to focus on the relative fractions of the populations, we fixed the age of the old population at 5 Gyr, and the metallicity of all populations at [Fe/H] $= -0.3$. These values equal the best-fitting mean age and metallicity found by Geha et al. (2003) in a study of Lick/IDS absorption line indices for dEs. Moreover, the spectra of SSPs of various ages do not differ much at ages of several Gyr and above (e.g. Bruzual & Charlot 2003).

The best fitting population was found by a χ^2 algorithm. In order to be able to calculate the χ^2 estimator, the observed and theoretical spectra have to be on the same wavelength grid (at least in the range used for the fit). This was done by rebinning the observed spectra to the resolution of the theoretical spectra using a gaussian kernel function with a full width at half maximum (FWHM) corresponding to the resolution of the theoretical spectra (20 Å for "BC99" and "Starburst", and 1 Å for "BC03"). The same was done with the "signal-to-noise spectra", i.e. the S/N as a function of wavelength provided along with the actual spectra. The χ^2 estimator was calculated with wavelength-dependent weighting, giving higher weight to the regions with a higher S/N. Fig. 9 shows an example of an observed spectrum and the resulting composite model spectra, as well as the individual spectra of the three assumed subpopulations.

5.3. *Fit to model spectra: results*

The best fitting population parameters for the fits with the different libraries can be found in columns 2 to 6 of Tables 4 to 6. In all dE(bc)s of the main sample, and all but one (VCC 1499) of the additional sample, the old population makes up for 90 % or more of the total mass, even though its contribution to the total light is rather small (spectra f_o in Fig. 9). The young population, on the other hand, usually contributes less than 1 % to the mass, but often dominates the light (f_y in Fig. 9), whereas the intermediate-age population usually makes up for a few percent of the stellar mass. However, all three populations are doubtlessly present, from which we conclude that these galaxies have been forming stars until the present day. We remind the reader again that the spectra cover only the very central part of our objects and do not allow us to draw direct conclusions about the surrounding regions.

Typically, the parameter space of such spectral fits is full of degeneracies. For example, a change of the ratio of the mass fractions of young and intermediate-age population has a similar effect on the composite spectrum as varying one of the ages of these populations. Therefore, the parameter values given in Tables 4 to 6 for *individual* galaxies should be taken with a grain of salt. However, the excellent agreement between the solutions found with the different libraries, and the similarities in the solutions for the different galaxies, suggest that the *general* trends in the derived parameters reflect the real properties of the dE(bc)s, within the simplified framework of our three-population models. We emphasize that our approach of approximating the SDSS spectra with synthetic populations composed of three SSPs is not meant to represent the detailed star formation history of our target galaxies, but only to demonstrate the range of ages during which star formation must have occured. Whether stars were formed by short starbursts or by extended episodes of star formation can typically not be decided for galaxies only observable in integrated light (e.g. Lilly & Fritze-v. Alvensleben 2003).

5.4. *Evolution of $g - i$ color*

Finally, we would like to know for how long after the last star formation phase integrated spectral properties can be distinguished from the ones of a pure old population. We focus on the $g - i$ color since it was used for the actual selection of our objects. For this purpose, we produced synthetic composite populations using the three SSP libraries, and calculated the total $g-i$ color as a function of the age of the youngest partial population as these composite populations evolve.

The simplest case is that of two populations: a young one turning into an intermediate-age one, on top of the old one. If we assume the mass of the young population to have one hundredth of the mass of the old one, the color of the mixture evolves as shown by the solid line in the upper panel of Fig. 10. In this scenario, it takes a few 100 Myr until the $g-i$ color of the composite population differs by less than 0.1 mag from a pure old population (shown by the dotted line), and thus becomes difficult to distinguish from the latter. The colors shown in Fig. 10 are the ones using the "BC99" library, but the results hold true for all three libraries.

Now we take instead a composite population like one of the typical solutions from Tables 4 to 6, that is, $(M_y + M_i){:}M_o = 1{:}10$, $M_y{:}M_i = 1{:}30$, the intermediate-age population being around 500 Myr older than the young one. $M_{y,i,o}$ denotes the mass fractions of young, intermediate-age, and old population, respectively. The color of this mixture evolves like the solid line in the lower panel of Fig. 10. Again, the dotted line shows the color of only an old population. In this scenario, the mixture is still distinguishable from a pure old population 500 Myr after the birth of the youngest one. However, this parameter combination is the one with the smallest mass fraction of the old population among the results for the main sample. By using the values of the other typical solutions from Tables 4 to 6, $(M_y+M_i){:}M_o = 1{:}30$, $M_y{:}M_i = 1{:}30$, or $(M_y + M_i){:}M_o = 1{:}100$, $M_y{:}M_i = 1{:}10$, the $g - i$ color after 500 Myr is much more similar to the pure old population color (big black dots in the lower panel of Fig. 10). Therefore, after the end of star formation it will take less than ∼ a Gigayear for the (strong) color gradient to disappear, and in many cases only ∼ half a Gigayear depending on the mass fraction of the young and intermediate-age population. This also demonstrates the need for a thorough study of both strong *and* weak color gradients in early-type dwarfs, in order to draw conclusions about evolutionary histories. Whether or not star formation will cease soon, or has ceased already in some objects, depends on the amount (and state) of leftover gas, which is the subject of the following section.

6. GAS CONTENT

Dwarf elliptical galaxies are commonly considered to be systems that have lost their (cold) gas (e.g. Ferguson & Binggeli 1994; Conselice et al. 2003). On the other hand, Conselice et al. (2003) reported "credible" HI detections for seven[6] Virgo dEs from their own study as well as from other literature, translating into a 15% HI detection rate for dEs.

---

[6] Two of these, however, were not classified as early-type dwarf in the VCC, and appear to us as at least doubtful dE candidates from visual inspection of the SDSS images.

The GOLDMine database (Gavazzi et al. 2003) reports detections for six more early-type dwarfs[7]. From the SDSS spectra presented above, we know that the dE(bc)s show clear signs of either ongoing or very recent star formation, suggesting the presence of a certain amount of gas. It would thus be interesting to know whether we can expect more episodes of star formation in the near future – requiring a significant cold gas content – or whether star formation is likely to cease soon due to the lack of leftover gas.

Two dE(bc)s of the main sample are detected in HI, while for 8 others, at least upper limits are available. Ten objects of the additional sample are detected in HI, and upper limits are available for three further galaxies. See Table 7 for HI masses and upper limits on our objects, along with the corresponding references to the literature. Two objects have values from more than one publication; these agree well within the errors.

We now seek to derive an estimate for the ratio of the gas mass to the total baryonic mass, $M_{\mathrm{HI}}/M_{\mathrm{bary}}$. For this purpose we use V-band mass-to-light ratios between 3 and 6, as given by Geha et al. (2003), and assume no dark matter content, again following Geha et al. (2003). We calculate the total V-band absolute magnitude from the g and i-band flux within an elliptical aperture with 1.5 times the estimated semi-major axis from Binggeli et al. (1985) (at $\sim \mu_{\mathrm{B}} = 25.5\mathrm{mag/arcsec}^2$), using the transformation of Smith et al. (2002). The resulting gas-to-baryonic mass fractions or upper limits for mass-to-light ratios of 3, 4.5, and 6 are listed in Table 7.

Of the dE(bc)s in the main sample, three objects have a very low gas content, with $M_{\mathrm{HI}}/M_{\mathrm{bary}}$ values of 1% or below (VCC 0170, VCC 0951, VCC 0953). Of the remaining galaxies, one has an HI content with a resulting fraction of $3-6\%$ (depending on the adopted mass-to-light ratio). The others have upper limits of several percent, up to $7-13\%$ for VCC 1488. In contrast, most of the galaxies in the additional sample have a much higher gas fraction. Of the 10 detected galaxies, 7 reach up to more than 10%, with values up to $38-55\%$. However, for one object (VCC 0135) the upper limit lies below 1%.

A comparison with average HI-to-total mass ratios for Local Group dwarf galaxies shows that at least some dE(bc)s of the main sample have a larger gas fraction than the $0.2 \pm 0.4\%$ of an ordinary dE, while it is mostly lower than the $30 \pm 24\%$ of dwarf irregulars (Conselice et al. 2003). If the detected gas was centrally concentrated, at least some of the dE(bc)s of the main sample might still continue to form stars there for a significant amount of time. In contrast, most objects of the additional sample fall in the range of the Local Group dIrrs, suggesting that a longer duration of star formation is possible. See Sect. 8 for a further discussion.

7. SYSTEMATIC PROPERTIES

We have shown so far that the dE(bc)s, which were classified morphologically as early-type dwarfs, are dominated by an old stellar population. Given their moderate amount of cold gas and the lack of any (significant) star formation activity beyond their central regions, the dE(bc)s will evolve into ordinary-looking dEs in the future. However, up to this point we have mainly focused on the appearance and the composition of the dE(bc)s, but we have not yet compared the statistical properties of the sample of dE(bc)s with those of the sample of dEs and dE(di)s (dEs with disks, see Sect. 3.2). As demonstrated in Paper I, the luminosity function, the projected spatial distribution, and the flattening distribution are important tools to investigate differences between types of galaxies, and to judge whether or not they constitute separate populations. We present and analyze these distributions for the dE(bc)s in the following subsections.

7.1. *Luminosity function*

Figure 11 shows the distribution of dE(bc)s, dE(di)s, and the remaining dEs with respect to their B band magnitude provided by the VCC. With the assumption that all galaxies are located at roughly the same distance from us, this distribution represents their luminosity function. Our data are presented as a running histogram with a bin-width of 1.0 mag (i.e. ±0.5 mag). Only galaxies with certain cluster membership are taken into account, i.e. 16 dE(bc)s in the main sample whose distribution is given by the dark grey shaded area. The dE(di)s are represented by the medium grey shaded area, and the full dE sample with dE(bc)s and dE(di)s excluded is given by the light grey shaded area. The fraction of dE(bc)s among the full dE sample is shown as black line. The white line shows the distribution of the 12 certain cluster members of the additional sample, which by construction are not included in the dE sample.

The luminosity function of the full dE sample is given as grey dashed line. It has a conspicuous bump at brighter magnitudes, which we explained in Paper I with the superposition of dE(di)s and ordinary dEs, implying that they were two different populations of objects. However, as can be seen in the figure, this bump might at least partly be explained by the superposition of dE(bc)s, dE(di)s, and the remaining dEs. On the other hand, it has been shown in Paper I that we missed ∼50% of dE(di)s due to issues of signal-to-noise. Therefore we now subtracted the dE(bc)s and 1.5 times the number of dE(di)s from the full sample as a further test (not shown). Still, there is no obvious over-subtraction of the bump (which would result in a dip), so the data are consistent with the estimated number of missed dE(di)s.

The fraction of dE(bc)s among all dEs reaches up to more than 15% for the main sample at brighter magnitudes, and declines to almost zero at $m_{\mathrm{B}} \gtrsim 16$. Thus the dE(bc)s are not a negligible population of objects, but instead constitute a significant fraction of the bright dEs. To investigate whether the decline of the dE(bc) fraction at fainter magnitudes is real or whether it is due to S/N effects, we artificially dimmed all 11 dE(bc)s of the main sample with $14 \leq m_{\mathrm{B}} < 15$ by 1 and 2 magnitudes. This was done by adding Gaussian noise to the images such that the RMS of the total noise was increased by 1 and 2 magnitudes. Color maps and radial color profiles were then constructed as described above, and were examined for whether they would have been selected as dE(bc)s by us. When dimmed by 1 magnitude, 9 of the 11 objects would still have been selected, whereas at 2 magnitudes fainter only 5 would have been recognized as dE(bc)s. Thus, if the *true* dE(bc) fraction would be constant at 17% (the average value within the interval $14 \leq m_{\rm B} < 15$) independent of magnitude, we would expect to *observe* a fraction of 14% at magnitudes between $15 \leq m_{\rm B} < 16$, and 8% between $16 \leq m_{\rm B} < 17$. Within these magnitude ranges, we should thus find 9.4 ± 2.8 and 8.2 ± 2.8 dE(bc)s, respectively, for a binomial distribution. However, we found only 4 and 0 dE(bc)s, which lies within 1.9 and 3.0 standard deviations, respectively. It is thus very likely that the decline of the number fraction of dE(bc)s is real.

---

[7] Three of these (VCC 0170, VCC 0227, VCC 0281) are listed as S0 or late-type spiral in the NASA/IPAC Extragalactic Database (NED) and similar in Gavazzi et al. (2005) who reported their HI detections, although they were classified as early-type dwarf in the VCC and confirmed as such by our Paper I.

Since we are using B band magnitudes, it is an obvious question how much fainter the dE(bc)s will become after their star formation has ceased. From our spectral analysis, we expect a decrease of the B band flux *of the central* $3''$ to one third of the current flux (median value: 0.32) for the main sample dE(bc)s. To obtain this estimate we compared the total spectrum of each galaxy with the model spectrum of the old population only, as a conservative estimate. Since our galaxies show a color gradient (Figs. 1 to 3), which we interpret as a decrease of the fraction of young stars when going outwards, we now assume that the above ratio of faded and current flux linearly increases to 1 up to the B band half-light radius. This leads to an estimated fading of the total galaxy flux in the B band of 0.2 mag for all dE(bc)s. Therefore, we do not expect significant evolution of the dE(bc) luminosity function after the cessation of star formation.

For the galaxies in the additional sample, Figs. 5 and 6 show that the blue regions are more extended. We therefore assume the linear increase of the ratio of faded and current flux (see above) to extend to two half-light radii. This leads to an estimated fading of $0.4 - 0.5$ mag. On average, these galaxies are already slightly fainter than the dE(bc)s of the main sample (see Fig. 11). This difference would thus become more pronounced after their star formation has ceased. On the other hand, one might expect from their gas content that a significant amount of stars could still be formed in these objects, which would counteract the fading to some extent.

7.2. *Flattening distribution*

The flattening distribution of the dE(bc)s is presented in Fig. 14, along with that of the dE(di)s from Paper I. The axial ratios were derived from the elliptical apertures provided by Paper I (see Sect. 4.1). Again, only galaxies with certain cluster membership are considered. The distributions are presented as running histograms with a binsize of 0.1 (±0.05), normalized to an area of 1. In the bottom right hand panel of the figure, we show various theoretical curves for comparison. We assume randomly distributed inclinations and oblate (black lines) or prolate (grey lines) intrinsic axial ratios. For the oblate case we adopt Gaussian distributions of various widths with a mean axial ratio of 0.4, while for the prolate case a mean value of 0.65 is used.

In Paper I, we deduced that dE(di)s are consistent with being flat oblate objects. Here, we find that the dE(bc)s of the main sample are similarly distributed, with slightly larger axial ratios than the dE(di)s. A comparison with the theoretical curves demonstrates that, despite the small sample size, their distribution is hardly consistent with dE(bc)s being spheroidal objects, and instead suggests the shape of a relatively thick disk. The galaxies of the additional sample are rounder, though not spheroidal. This is another point – besides the overall gas content, strength of emission lines, and size of star forming regions – in which the dE(bc)s of the main sample and the additional galaxies are not alike.

7.3. *Spatial distribution*

In Paper I we found that while ordinary dEs are more strongly clustered towards the Virgo cluster center, dE(di)s basically show no clustering at all, another indication for them being a different population of galaxies. The dE(bc)s of the main sample also show no central clustering (Fig. 12, upper panel), similar to the dE(di)s. The same applies to the objects of the additional sample (Fig. 12, lower panel). While the number of dE(bc)s is relatively small and does not allow statistically secure statements, their distribution is hardly consistent with a centrally concentrated population.

7.4. *Morphology-density relation*

In Fig. 13 we present the cumulative distributions of projected local densities – calculated as in Dressler (1980) and Binggeli et al. (1987) – for the dE(bc)s, the galaxies of the additional sample, the dE(di)s, and the remaining, ordinary dEs (upper panel). We also compare these with the distributions of standard Hubble types (lower panel), i.e., with the well-known morphology-density relation.

The dE(bc)s and the objects of the additional sample are preferentially found in regions of moderate to lower density, and are distributed similarly to the irregular galaxies. This implies that they, as a population, are far from being virialized, corroborating the indications from the spatial distribution (Sect. 7.3). The dE(di)s show a similar distribution, which follows that of the spiral galaxies. Ordinary dEs, though, are preferentially found in higher density regions. Their location in the morphology-density diagram is intermediate between E/S0 galaxies and spirals.

7.5. *Velocity distribution*

Heliocentric velocities are available for 194 early-type dwarfs of our full dE sample that are certain Virgo cluster members (see Sect. 2.3). We present these data in Fig. 15 for the dE(bc)s, the dE(di)s, and the remaining dEs (i.e., dE(bc)s and dE(di)s excluded). Each panel shows a running histogram with a bin-width of 366 km $\rm s^{-1}$, which corresponds to the semi-interquartile range of all 194 velocities. Their median value, $v_{\rm helio} = 1248$ km $\rm s^{-1}$, is given as a dotted vertical line in each panel for comparison.

The dE(bc)s of the main sample show a relatively large deviation from the overall median value: their median velocity is only $v_{\rm helio} = 802$ km $\rm s^{-1}$. However, since the semi-interquartile range is large ($\Delta v_{\rm helio} = 463$ km $\rm s^{-1}$), and since only 15 objects are included in this sample, we cannot state whether this constitutes a significant difference. Instead, it might be more promising to compare the shapes of the distributions. The sample of ordinary dEs shows a close-to-symmetric distribution, which would be expected for a relaxed population. In contrast, the distribution of dE(bc)s and dE(di)s are asymmetric and less smooth. Both display side peaks, indicative of an infalling population (Tully & Shaya 1984; Conselice et al.

2001). This would be consistent with their spatial distribution, which shows no central concentration within the cluster, and with their distribution with projected local density, which follows that of the irregular cluster galaxies.

8. DISCUSSION

The SDSS enables for the first time a systematic study of several hundred dEs in the Virgo cluster with optical imaging and partly with spectroscopy. These data provide the basis for this series of papers, which aims at disentangling the various subpopulations of early-type dwarfs and uncovering their evolutionary histories. In Paper I, we found that dEs with disk features (dE(di)s) constitute a disk-shaped, unrelaxed dE population that is clearly different from classical dwarf ellipticals. In the current paper, we focus on another conspicuous feature that is common to several dEs: a blue center caused by recent or ongoing central star formation. We have shown that these dE(bc)s constitute a significant fraction (more than 15%) of bright dEs in the Virgo cluster. This number declines to almost zero beyond $m_{\rm B} > 16$, which is most likely a real decline and is not mainly due to signal-to-noise effects.

Two dE(bc)s of the main sample are detected in HI, with gas-to-baryonic mass fractions of 1% and $3-6$%, respectively. These values and the upper limits for several other dE(bc)s suggest an average gas content larger than that of ordinary dEs, but lower than that of dwarf irregulars. Note that we do not know where in the galaxies the gas is located: if it were concentrated in the central region, it would probably be able to fuel star formation for a longer time than if the gas were distributed homogeneously.

As soon as star formation has ceased, each dE(bc)'s color – which provided the basis of its selection – will become indistinguishable from that of an ordinary dE within $\sim$ a Gigayear or less (see Sect. 5.4). However, the statistical properties of the dE(bc) *population* are unlike those of ordinary dEs: the projected spatial distribution and the flattening distribution of the dE(bc)s are similar to those of the dE(di)s and are different from those of dEs that have no blue centers or disk features. Both the dE(bc) and dE(di) population show no central clustering, which, along with the side-peaks of their velocity distributions, hints towards fairly recent infall. How long ago this infall could have taken place depends on relaxation timescales. Conselice et al. (2001) derived a two-body relaxation time for the Virgo dEs of much more than a Hubble time. Even violent relaxation, which might only apply for the case of merging groups or subclusters, would take at least a few crossing times $t_{\rm cr}$, with $t_{\rm cr} \approx 1.7$ Gyr for the Virgo cluster (Boselli & Gavazzi 2006). Thus, a dE population built out of infalling galaxies remains in an unrelaxed, non-virialized state for many Gyr. We conclude that the dE(bc)s most likely formed through infall of progenitor galaxies.

The shape of the dE(bc)s, as deduced from their flattening distribution, is hardly consistent with their being spheroidal objects, and instead implies that the dE(bc)s are rather thick disks, i.e. oblate-shaped objects with intrinsic axial ratios around $\sim$0.4. This is only somewhat thicker than the dE(di)s, for which we derived an axial ratio of $\sim$0.35 in Paper I. How could these disk-shaped dEs be produced?

8.1. *Formation scenarios*

In the galaxy harassment scenario (Moore et al. 1996), an infalling late-type disk galaxy gets transformed into a dE through high-speed encounters with massive cluster galaxies. This obviously leads to an increase in the axial ratio during the transformation process, since a disk is converted into a spheroid. However, a thick stellar disk may survive and lead to lenticular systems (Moore et al. 1996; Mastropietro et al. 2005). These may form a bar and spiral features, and retain them for some time, depending on the tidal heating of the galaxy (Mastropietro et al. 2005). Galaxy harassment thus appears to be a plausible scenario to explain the formation of disk-shaped dEs, and of dE(di)s in particular. Moreover, it predicts gas to be funneled to the center and form a density excess there (Moore et al. 1998). While Moore et al. compare this to the presence of a nucleus in many dEs, they admit that their simulations "were not designed to probe the inner 200 pc". The radii of many of the blue central regions of the dE(bc)s are only slightly larger than this value (see Figs. 1 to 3); consequently, the central gas density excess could well explain the blue centers. The harassment scenario thus describes a possible evolution of an infalling late-type disk galaxy to a dE(bc) and to a dE(di).

Another mechanism to form disk-shaped dEs could be ram-pressure stripping (e.g. Gunn & Gott 1972) of dwarf irregulars. Depending on galaxy mass, the gas might be significantly removed except around the central region (Mori & Burkert 2000), which would seem to be consistent with the central star formation of the dE(bc)s. As shown by van Zee et al. (2004), several dEs have significant rotation, and could thus be the descendants of dIrrs, which are also known to be mostly rotationally supported, at least at the luminosities considered here. However, apart from the problems with this scenario discussed in Sect. 1, like the metallicity offset between dEs and dIrrs or the too strong fading of dIrrs, the flattening distribution of dIrrs shown by Binggeli & Popescu (1995) is not quite like that of our dE(bc)s. Instead, dIrrs have a (primary) axial ratio $\geq$0.5. On the other hand, significant mass loss due to stripped gas would be expected to affect also the *stellar* configuration of the galaxies and could thus possibly account for the difference.

As outlined in Sect. 1, several studies claimed that BCDs might be progenitors of dEs. Their flattening distribution, as analyzed by Binggeli & Popescu (1995), is somewhat more like that of our dE(bc)s, though still slightly rounder. These BCDs behave similarly to the galaxies of our additional sample – which were mostly classified as (candidate) BCDs, but were selected only if their appearance was similar to the dE(bc)s. Overall, they have more extended blue regions, stronger emission lines, and clearly a higher gas content than the dE(bc)s of the main sample. They are also dominated by an underlying old population – only one out of seven has $M_{\rm old} < 90\%$ – and they have fairly regular outer shapes. Their spatial distribution also hints at an unrelaxed population, and their velocity distribution is asymmetric.

Tidally induced star formation in dIrrs (Davies & Phillipps 1988) might be able to link BCDs and dEs, and could at the same time overcome the problems of the ram-pressure stripping scenario. The initially lower metallicity and surface brightness of a dIrr are increased by several bursts of star formation, during which the galaxy appears as blue compact dwarf (BCD). After that, it fades to become a dE. The last star formation burst might occur in the central region of the dwarf (Davies & Phillipps 1988), consistent with the appearance of the dE(bc)s.

8.2. *Presence of nuclei*

Many late-type spirals – which act as dE progenitors in the harassment scenario – host a compact nucleus (e.g. Böker et al. 2004). If the nucleus survives the morphological transformation, it would become the nucleus of the resulting dE(bc) or dE(di). A second scenario for nucleus formation in dEs is late star formation out of central gas (e.g. Oh & Lin 2000), which in principle might be taking place in the centers of the dE(bc)s.

The fraction of nucleated galaxies among the dE(bc)s is 7/16 (44%), which is based on the VCC classification and has been verified by us through visual inspection of images and unsharp masks. We find one more dE(bc) to have "multiple nuclei" (VCC 0021), and one to have a possible nucleus (VCC 1512). If those two objects were counted as being nucleated, the fraction would increase to 56%. Among the dE(di)s, 26 out of 36 galaxies are nucleated (72%). Ordinary dEs (i.e. excluding dE(bc)s and dE(di)s) have a nucleated fraction of also 72% among the brighter objects ($m_{\rm B} \leq 16$), which is the magnitude range of most dE(di)s and of all but one dE(bc). If we assumed a 72% nucleated fraction for the dE(bc)s as well, we would expect to find 11.5 nucleated dE(bc)s among our 16 objects, with a standard deviation $\sigma = 1.8$. Our observed number thus lies within 1.4σ of the expected value if dE(bc)s had the same nucleated fraction as dEs and dE(di)s, and if the two uncertain objects were counted as nucleated. Thus, there is no significant difference between dE(bc)s, dE(di)s, and the other dEs with respect to the presence or absence of a nucleus. Still, the somewhat smaller number of nuclei in dE(bc)s could be a hint that nuclei are indeed forming in their centers. Of the galaxies in the additional sample, none displays a nucleus, but the significant amount of central gas and dust might leave the possibility of a hidden nucleus, or of a nucleus just being formed.

We point out that the ACS Virgo Cluster Survey (Côté et al. 2004) finds a much higher frequency of compact stellar nuclei in early-type galaxies than Binggeli et al. (1985) did, primarily due to the much higher resolution of space-based studies as compared to ground-based ones (Côté 2005). However, if we took into account these results, a dE classified as nucleated in the VCC would then simply be termed *a dE with a nucleus bright enough to have been detected by Binggeli et al. (1985).*

8.3. *Presence of dE(bc)s in less dense environments*

Early-type dwarfs with blue centers are not only present in the Virgo cluster. NGC 205, with its central region of young stars and central dust clouds (Hodge 1973), is a well known local example of what we term a dE(bc); the same applies to NGC 185 (Hodge 1963). On the one hand, NGC 205 might be considered as special case due to its clear signs of tidal interaction with M 31 (Mateo 1998). On the other hand, tidal interaction might not be something special but instead something very common and even required for the formation of dEs, and of dE(bc)s in particular. While galaxy harassment is negligible in groups (Mayer et al. 2001b), a similar mechanism is provided there by the so-called tidal stirring scenario (Mayer et al. 2001a), in which a dIrr that suffers repeated tidal shocks is transformed into a dE or a dSph. In this model, the galaxies with higher surface brightness can reach a central gas density excess like what was described above for harassment. Tidal stirring might thus provide a consistent explanation for dE(bc)s in groups.

Contrary to the above interpretation of NGC 185 and NGC 205 as possible result of tidal stirring, Gu et al. (2006) recently presented an apparently isolated dwarf elliptical with a blue center (IC 225) at a distance of 20.6 Mpc. Its spectrum displays Balmer line emission, and based on its appearance it would doubtlessly enter our dE(bc) sample. The authors base their conclusion about the galaxy's isolation on their failure to find a potential companion within 30 arcmin, using the NED. This angular search radius corresponds to 180 kpc at their given distance. We increased the search radius, and found the small galaxy group USGC U124 (Ramella et al. 2002) to lie at the same distance as IC 225 (within 25 km s^{-1} in radial velocity), and at an angular separation of 145 arcmin, or 870 kpc. The brightest group member (NGC 0936) is an early-type spiral galaxy with $M_{\rm B} \approx -20.5$. Since 870 kpc would seem a rather large distance for IC 225 to be a bound companion, we test whether a single interaction could have occured in the past. As an example, if the relative velocity was 100 km s^{-1}, the encounter would have occured 8.5 Gyr ago, much too long for the current star formation to have been triggered by it.

While the tidal forces of smaller galaxies closer to IC 225 could possibly affect the galaxy's gas distribution, Brosch et al. (2004) argued that tidal interactions might not be necessary for activating star formation, and that instead, the dynamics of gas masses in a dark matter gravitational potential could be the primary trigger. Nevertheless, the main problem would be to explain how an *isolated dE* could have formed at all. Therefore, if IC 225 is indeed a truly isolated galaxy, one has to think of other mechanisms for dE formation than the ones we have discussed. It also demonstrates along with NGC 185 and NGC 205 that central star formation does not only occur in cluster dEs, and that, consequently, the mechanisms for dE formation might be similar in different environments. In fact, in the Local Group, where we can study galaxies at the highest angular resolution, many dSphs show star formation histories that extend over many Gyr. In all of these cases, the younger populations are more centrally concentrated than the old ones (Harbeck et al. 2001). Apart from interactions, this may also be a consequence of longer-lived gas reservoirs at the centers of these galaxies' potential wells.

Finally, we caution against calling the dE(bc)s "dE/dIrr transition types": this would suggest that every dE(bc) has a dIrr progenitor, which might not be the case as discussed above. Similarly, Grebel et al. (2003) argued for Local Group dwarfs that the so-called dIrr/dSph transition types are plausible progenitors of dSphs, while dIrrs themselves seem less likely.

9. SUMMARY AND OUTLOOK

We have presented a study of Virgo cluster early-type dwarf galaxies (dEs) with central star forming regions, based on photometric and spectroscopic data from the SDSS DR4. These "dE(bc)s" are not rare objects, but they reach a fraction of more than 15% among the bright ($m_{\rm B} < 16$) dEs. Their spatial distribution and their distribution with projected local density suggest that they are an unrelaxed population. Their flattening distribution is consistent with them being disk-shaped objects like the dEs with disk substructure (dE(di)s) identified in Paper I. Even in the very center, where their colors are bluest, 90% or more of their mass belongs to an old stellar population. Thus, they will appear like ordinary dEs within about one Gigayear after the end of their star formation. The gas content of the dE(bc)s is lower than in dwarf irregulars, but probably somewhat higher than in classical dEs, implying that at least in some dE(bc)s star formation might still continue for some time. Plausible formation mechanisms that could explain both the disk shape and the central star formation of the dE(bc)s are galaxy harassment (Moore et al. 1996), which describes the transformation of infalling late-type disk galaxies into dEs, tidally induced star formation in dIrrs (Davies & Phillipps 1988), and possibly also ram-pressure stripping (Gunn & Gott 1972) of dIrrs and star formation induced by gas compression due to ram pressure.

We have started our series of papers on Virgo early-type dwarfs by describing two sorts of dEs with "special features", i.e., dEs with a blue center (this study) and dEs with disk substructure (Paper I). It is important to stress that we are not looking at one single population of dEs, with those features just being some extra "flavour", but that these dE subtypes constitute populations with distinct properties that differ from the rest of dEs. To complicate the issue even more, ordinary dEs (i.e., exluding dE(bc)s and dE(di)s) are probably not a homogeneous population either, since e.g. the clustering properties of nucleated and non-nucleated dEs differ significantly (Binggeli et al. 1987). Whether or not all of these dE subtypes simply reflect different evolutionary stages of one single class of galaxy, or whether they are indeed different classes of early-type dwarfs, will be discussed in detail in a forthcoming paper.

It is a pleasure to thank B. Binggeli for many fruitful discussions and a careful reading of the manuscript. We thank the referee for useful comments that helped us improve the paper. We gratefully acknowledge support by the Swiss National Science Foundation through grants number 200020-105260, 200020-105535, and 200021-109616. We thank J. Gallagher for stimulating discussions.

This study would not have been possible without the wealth of publicly available data from the SDSS Data Release 4, or without the fantastic work of those who created and maintain the SDSS webpages. Funding for the SDSS has been provided by the Alfred P. Sloan Foundation, the Participating Institutions, the National Science Foundation, the U.S. Department of Energy, the National Aeronautics and Space Administration, the Japanese Monbukagakusho, the Max Planck Society, and the Higher Education Funding Council for England. The SDSS Web Site is http://www.sdss.org/.

The SDSS is managed by the Astrophysical Research Consortium for the Participating Institutions. The Participating Institutions are the American Museum of Natural History, Astrophysical Institute Potsdam, University of Basel, Cambridge University, Case Western Reserve University, University of Chicago, Drexel University, Fermilab, the Institute for Advanced Study, the Japan Participation Group, Johns Hopkins University, the Joint Institute for Nuclear Astrophysics, the Kavli Institute for Particle Astrophysics and Cosmology, the Korean Scientist Group, the Chinese Academy of Sciences (LAMOST), Los Alamos National Laboratory, the Max-Planck-Institute for Astronomy (MPIA), the Max-Planck-Institute for Astrophysics (MPA), New Mexico State University, Ohio State University, University of Pittsburgh, University of Portsmouth, Princeton University, the United States Naval Observatory, and the University of Washington.

This research has made use of NASA's Astrophysics Data System Bibliographic Services, and of the NASA/IPAC Extragalactic Database (NED) which is operated by the Jet Propulsion Laboratory, California Institute of Technology, under contract with the National Aeronautics and Space Administration. This research has also made use of the GOLDMine Database.

REFERENCES

Adelman-McCarthy, J. K., Agüeros, M. A., Allam, S. S., et al. 2006, ApJS, 162, 38
Binggeli, B. 1985, in Star-Forming Dwarf Galaxies and Related Objects, ed. D. Kunth, T. X. Thuan, & J. Tran Thanh van, 53
Binggeli, B., & Cameron L., M. 1991, A&A, 252, 27
Binggeli, B. & Cameron, L. M. 1993, A&AS, 98, 297
Binggeli, B. & Popescu, C. C. 1995, A&A, 298, 63
Binggeli, B., Popescu, C. C., & Tammann, G. A. 1993, A&AS, 98, 275
Binggeli, B., Sandage, A., & Tammann, G. A. 1985, AJ, 90, 1681
Binggeli, B., Tammann, G. A., & Sandage, A. 1987, AJ, 94, 251
Böker, T., Walcher, C. J., Rix, H. W., et al. 2004, in ASP Conf. Ser. 322: The Formation and Evolution of Massive Young Star Clusters, ed. H. J. G. L. M. Lamers, L. J. Smith, & A. Nota, 39
Boselli, A. & Gavazzi, G. 2006, PASP, 118, 517
Boselli, A., Iglesias-Páramo, J., Vílchez, J. M., & Gavazzi, G. 2002, A&A, 386, 134
Bothun, G. D., Mould, J. R., Caldwell, N., & MacGillivray, H. T. 1986, AJ, 92, 1007
Brosch, N., Almoznino, E., & Heller, A. B. 2004, MNRAS, 349, 357
Bruzual A., G., & Charlot, S. 1993, ApJ, 405, 538
Bruzual A., G., & Charlot, S. 2000, Galaxy isochrone spectral synthesis evolution library (private communication)
Bruzual A., G., & Charlot, S. 2003, MNRAS, 344, 1000
Caldwell, N., Rose, J. A., & Concannon, K. D. 2003, AJ, 125, 2891
Calzetti, D., Armus, L., Bohlin, R. C., et al. 2000, ApJ, 533, 682
Charbonnel, C., Maeder, A., Schaller, G., et al. 1993, A&AS, 101, 415
Charlot, S., & Bruzual A., G. 1991, ApJ, 367, 126
Cid Fernandes, R., Leão, J. R. S., & Lacerda, R. R. 2003, MNRAS, 340, 29
Conselice, C. J., Gallagher, III, J. S., & Wyse, R. F. G. 2001, ApJ, 559, 791
Conselice, C. J., O'Neil, K., Gallagher, J. S., & Wyse, R. F. G. 2003, ApJ, 591, 167
Côté, P. 2005, in IAU Colloq. 198: Near-field cosmology with dwarf elliptical galaxies, ed. H. Jerjen & B. Binggeli (Cambridge: CUP), 269–276
Côté, P., Blakeslee, J. P., Ferrarese, L., et al. 2004, ApJS, 153, 223

Cuisinier, F., Westera, P., Telles, E., & Buser, R. 2006, A&A, 423, 133

Davies, J. I. & Phillipps, S. 1988, MNRAS, 233, 553

de Vaucouleurs, G., de Vaucouleurs, A., Corwin, Jr., H. G., et al. 1991, Third Reference Catalogue of Bright Galaxies (Volume 1-3, XII, 2069 pp., Springer-Verlag Berlin Heidelberg New York)

Dressler, A. 1980, ApJ, 236, 351

Drinkwater, M. J., Currie, M. J., Young, C. K., Hardy, E., & Yearsley, J. M. 1996, MNRAS, 279, 595

Fagotto F., Bressan A., Bertelli G., & Chiosi C., 1994 A&AS 105, 29

Falco, E. E., Kurtz, M. J., Geller, M. J., et al. 1999, PASP, 111, 438

Ferguson, H. C. & Binggeli, B. 1994, A&A Rev., 6, 67

Ferrarese, L., Cote, P., Jordan, A., et al. 2006, ApJS, 164, 334

Ferrarese, L., Mould, J. R., Kennicutt, Jr., R. C., et al. 2000, ApJ, 529, 745

Fluks, M. A., Plez, B., Thé, P. S., et al. 1994, A&AS, 105, 311

Gavazzi, G., Bonfanti, C., Pedotti, P., Boselli, A., & Carrasco, L. 2000, A&AS, 146, 259

Gavazzi, G., Boselli, A., Donati, A., Franzetti, P., & Scodeggio, M. 2003, A&A, 400, 451

Gavazzi, G., Boselli, A., van Driel, W., & O'Neil, K. 2005, A&A, 429, 439

Gavazzi, G., Zaccardo, A., Sanvito, G., Boselli, A., & Bonfanti, C. 2004, A&A, 417, 499

Geha, M., Guhathakurta, P., & van der Marel, R. P. 2003, AJ, 126, 1794

Girardi, L., Bressan, A., Chiosi, C., Bertelli, G., & Nasi, E. 1996, A&AS, 117, 113

Girardi, L., Bressan, A., Bertelli, G., & Chiosi, C. 2000, A&AS, 141, 371 ("Padova 2000" isochrones)

Grebel, E. K. 2001, Astrophysics and Space Science Supplement, 277, 231

Grebel, E. K., Gallagher, J. S., & Harbeck, D. 2003, AJ, 125, 1926

Grogin, N. A., Geller, M. J., & Huchra, J. P. 1998, ApJS, 119, 277

Gu, Q., Zhao, Y., Shi, L., Peng, Z., & Luo, X. 2006, AJ, 131, 806

Gunn, J. E. & Gott, J. R. I. 1972, ApJ, 176, 1

Gunn, J. E., Carr, M., Rockosi, C., et al. 1998, AJ, 116, 3040

Guzman, R., Koo, D. C., Faber, S. M., et al. 1996, ApJ, 460, L5

Harbeck, D., Grebel, E. K., Holtzman, J., et al. 2001, AJ, 122, 3092

Hodge, P. W. 1973, ApJ, 182, 671

Hodge, P. W. 1963, AJ, 68, 691

Huchtmeier, W. K. & Richter, O.-G. 1989, A&A, 210, 1

Huchtmeier, W. K. & Richter, O.-G. 1986, A&AS, 64, 111

Jerjen, H., Kalnajs, A., & Binggeli, B. 2000, A&A, 358, 845

Johnson, R. A., Lawrence, A., Terlevich, R., & Carter, D. 1997, MNRAS, 287, 333

Knezek, P. M., Sembach, K. R., & Gallagher, J. S. 1999, ApJ, 514, 119

Kniazev, A. Y., Pustilnik, S. A., Grebel, E. K., Lee, H., & Pramskij, A. G. 2004, ApJS, 153, 429

Kong, X., Charlot, S., Weiss, A., & Cheng, F. 2003, A&A, 403, 877

Le Borgne, J.-F., Bruzual A., G., Pelló, R., et al. 2003, A&A, 402, 433

Leitherer, C., Schaerer, D., Goldader, J. D., et al. 1999, ApJS, 123, 3

Lejeune, T., Cuisinier, F., & Buser, R. 1997, A&AS, 125, 229

Lejeune, T., Cuisinier, F., & Buser, R. 1998, A&AS, 130, 65

Lilly, T. & Fritze-v. Alvensleben, U. 2004, in IAU Symp. 221: Star Formation at High Angular Resolution, ed. M. Burton, R. Jayawardhana, & T. Bourke, 80

Lisker, T., Grebel, E. K., & Binggeli, B. 2005, in IAU Colloq. 198: Near-field cosmology with dwarf elliptical galaxies, ed. H. Jerjen & B. Binggeli (Cambridge: CUP), 311

Lisker, T., Grebel, E. K., & Binggeli, B. 2006, AJ, 132, 497, *Paper I*

Maraston, C. 2005, MNRAS, 362, 799

Mastropietro, C., Moore, B., Mayer, L., et al. 2005, MNRAS, 364, 607

Mateo, M. L. 1998, ARA&A, 36, 435

Mayer, L., Governato, F., Colpi, M., et al. 2001b, ApJ, 559, 754

Mayer, L., Governato, F., Colpi, M., et al. 2001a, ApJ, 547, L123

Meynet, G., Maeder, A., Schaller, G., Schaerer, D., & Charbonnel, C. 1994, A&AS, 103, 97

Moore, B., Katz, N., Lake, G., Dressler, A., & Oemler, A. 1996, Nature, 379, 613

Moore, B., Lake, G., & Katz, N. 1998, ApJ, 495, 139

Mori, M. & Burkert, A. 2000, ApJ, 538, 559

Oh, K.S. & Lin, D., N., C. 2000, ApJ, 543, 620

Osterbrock, D. E. 1989, Astrophysics of Gaseous Nebulae and Active Galactic Nuclei (Mill Valley: University Science Books)

Papaderos, P., Loose, H.-H., Fricke, K. J., & Thuan, T. X. 1996, A&A, 314, 59

Pier, J. R., Munn, J. A., Hindsley, R. B., et al. 2003, AJ, 125, 1559

Rakos, K. & Schombert, J. 2004, AJ, 127, 1502

Ramella, M., Geller, M. J., Pisani, A., & da Costa, L. N. 2002, AJ, 123, 2976

Richer, M., McCall, M. L., & Stasinska, G. 1998, A&A, 340, 67

Ryden, B. S. & Terndrup, D. M. 1994, ApJ, 425, 43

Sandage, A. & Binggeli, B. 1984, AJ, 89, 919

Schaerer, D., Charbonnel, C., Meynet, G., Maeder, A., & Schaller, G. 1993a, A&AS, 102, 339

Schaerer, D., Meynet, G., Maeder, A., & Schaller, G. 1993b, A&AS, 98, 523

Schaller, G., Schaerer, D., Meynet, G., & Maeder, A. 1992, A&AS, 96, 269

Schlegel, D. J., Finkbeiner, D. P., & Davis, M. 1998, ApJ, 500, 525

Schmutz, W., Leitherer, C., & Gruenwald, R. 1992, PASP, 104, 1164

Simien, F. & Prugniel, P. 2002, A&A, 384, 371

Smith, J. A., Tucker, D. L., Kent, S., et al. 2002, AJ, 123, 2121

Stoughton, C., Lupton, R. H., Bernardi, M., et al. 2002, AJ, 123, 485

Strauss, M. A., Huchra, J. P., Davis, M., et al. 1992, ApJS, 83, 29

Thuan, T. X. 1985, ApJ, 299, 881

Tody, D. 1993, in ASP Conf. Ser. 52, Astronomical Data Analysis Software and Systems II, ed. R. J. Hanisch, R. J. V. Brissenden, and J. Barnes (San Francisco: ASP), 173

Torres-Peimbert, S., Peimbert, M., & Fiero, J. 1989, ApJ, 345, 186

Tully, R. B. & Shaya, E. J. 1984, ApJ, 281, 31

van Driel, W., Ragaigne, D., Boselli, A., Donas, J., & Gavazzi, G. 2000, A&AS, 144, 463

van Zee, L., Skillman, E. D., & Haynes, M. P. 2004, AJ, 128, 121

Vigroux, L., Souviron, J., & Vader, J. P. 1984, A&A, 139, L9

Westera, P. 2001, The BaSeL 3.1 models: Metallicity calibration of a theoretical stellar spectral library and its application to chemodynamical galaxy models, PhD thesis, Univ. of Basel, 378 pp.

Westera, P., Lejeune, T., Buser, R., Cuisinier, F., & Bruzual A., G. 2002, A&A, 381, 524

Westera, P., Cuisinier, F., Telles, E., & Kehrig, C. 2004, A&A, 423, 133

York, D. G., Adelman, J., Anderson, J. E., et al. 2000, AJ, 120, 1579

Young, C. K. & Currie, M. J. 1995, MNRAS, 273, 1141

TABLE 1
Early-type dwarfs with blue centers.

VCC	α_{J2000}	δ_{J2000}	Mem.	m_{B} (mag)	Class	Note
Main sample						
0021	$12^{\mathrm{h}}10^{\mathrm{m}}23\overset{\mathrm{s}}{.}2$	$+10^{\circ}11'19''$	M	14.75	dS0(4)	
0046	12 12 11.0	+12 53 37	P	17.00	dE3?	S
0170	12 15 56.3	+14 26 00	M	14.86	dS0 pec:	
0173	12 16 00.4	+08 12 08	M	15.00	dS0(1)?	
0218	12 17 05.4	+12 17 22	M	14.88	dS0(8),N:	D2
0278	12 18 14.4	+06 36 14	P	15.10	dS0,Npec	D1s
0281	12 18 15.2	+13 44 58	M	15.30	dS0 or BCD	S, H$\alpha\beta$
0308	12 18 50.9	+07 51 43	M	14.30	d:S0_1(0),N:	D1s
0636	12 23 21.3	+15 52 06	P	16.44	dE0,N or S0_1(0)	
0674	12 23 52.6	+13 52 58	M	18.00	dE0,N	
0781	12 25 15.2	+12 42 53	M	14.46	dS0_3(5),N:	S, Hα
0870	12 26 05.4	+11 48 43	M	14.68	dS0(5),N	S, H$\alpha\beta$
0951	12 26 54.4	+11 39 50	M	14.23	dE2 pec,N or dS0(2),N	S, Hα
0953	12 26 54.8	+13 33 58	P	15.70	dE5?,Npec?	S
1078	12 28 11.4	+09 45 38	P	15.30	dE5 pec?	S, Hα
1488	12 33 13.5	+09 23 51	M	14.76	dE:	S; *Hα lit.*
1501	12 33 24.7	+08 41 27	M	15.10	dS0?	
1512	12 33 34.6	+11 15 43	M	15.73	dS0 pec	
1617	12 35 30.9	+06 20 01	P	15.00	d:S0(4) pec?	
1684	12 36 39.4	+11 06 07	M	14.87	dS0(8):	S, Hα; D3
1715	12 37 28.5	+08 47 40	P	16.20	dE0 pec?	
1779	12 39 04.7	+14 43 52	M	14.83	dS0(6):	D3
1912	12 42 09.1	+12 35 48	M	14.16	dS0(8),N	
Additional sample						
0024	12 10 35.7	+11 45 39	M	14.95	BCD	S, H$\alpha\beta$
0135	12 15 06.9	+12 00 59	M	14.81	S pec / BCD	S, H$\alpha\beta$
0334	12 19 14.2	+13 52 57	M	16.20	BCD	
0340	12 19 22.1	+05 54 38	P	14.43	BCD or merger	S, H$\alpha\beta$
0446	12 20 57.9	+06 20 21	M	15.50	Im / BCD:	
0841	12 25 47.6	+14 57 07	M	16.70	BCD	
0890	12 26 21.6	+06 40 11	P	16.00	BCD?	
1175	12 29 18.5	+10 08 13	M	15.10	E5 / S0_1(5)	S, H$\alpha\beta$; M32
1273	12 30 17.0	+09 05 07	M	15.25	ImIII:	S, H$\alpha\beta$
1437	12 32 33.5	+09 10 25	M	15.70	BCD	S, H$\alpha\beta$
1499	12 33 20.2	+12 51 04	M	14.58	E3 pec or S0	S
1955	12 43 07.6	+12 03 00	M	14.12	S pec / BCD	*Hα lit.*
2007	12 44 47.5	+08 06 25	M	15.20	ImIII / BCD:	*Hα lit.*
2033	12 46 04.4	+08 28 34	M	14.65	BCD	*Hα lit.*

Note. — Cluster membership (column “Mem.”) is provided by Binggeli et al. (1985, 1993): M = certain cluster member, P = possible member. Classification as in the VCC, except for VCC 1488 which has been reclassified as probable dE by Geha et al. (2003) (former class E6:). VCC 1175 belongs to the M32-like compact ellipticals (Binggeli et al. 1985). Notes in the last column are as follows: D = disk identified in Paper I, D1s = certain disk with spiral arms, D2 = probable disk, D3 = possible disk. S = useful spectrum available. H$\alpha\beta$ = spectrum displays Balmer line emission; Hα = spectrum displays only Hα emission. *Hα lit.* = Hα detection reported by Boselli et al. (2002). Only given if Hα is not detected in the SDSS spectrum, or if no spectrum was available. Units of right ascension are hours, minutes, and seconds, and units of declination are degrees, arcminutes, and arcseconds.

TABLE 2
Wavelength ranges that were not used for the spectral fit.

range (Å)	"contamination" source
3885-3900	H8
3965-3980	Hϵ+[NeIII]3967
4100-4110	Hδ
4335-4345	Hγ+[OIII]4363
4855-4870	Hβ
4955-4965	[OIII]4959
5000-5015	[OIII]5007
5535-5590	telluric lines
5860-5905	HeI 5876
6245-6320	[OI]6300+[SIII]6312
6520-6600	Hα+[NII]
6700-6740	[SII]6717+6731
7130-7145	[ArIII]7136
7560-7600	telluric lines
7700-8100	telluric lines
8250-8480	telluric lines

TABLE 3
Possible values of the population parameters.

parameter	possible values
$(M_y + M_i)$:M_o	0:1, 1:100, 1:30, 1:10, 1:3, 1:1, 3:1, 10:1, 1:0
M_y:M_i	0:1, 1:30, 1:10, 1:3, 1:1, 3:1, 10:1, 30:1, 1:0
age_y	1, 2, 3, 4, 5, 6, 7, 8, 9 Myr
age_i	10, 20, 50, 100, 200, 500 Myr
age_o	fixed at 5 Gyr
$[\mathrm{Fe/H}]_y$	fixed at -0.3
$[\mathrm{Fe/H}]_i$	fixed at -0.3
$[\mathrm{Fe/H}]_o$	fixed at -0.3

Note. — The young population is denoted by index y, the intermediate-age one by i and the old one by o. M_x is the mass fraction of the respective population.

TABLE 4
Best fitting parameters using the "BC99" library.

VCC	M_y	age_y	M_i	age_i	M_o
Main sample					
0021	0.0029	9 Myr	0.0880	509 Myr	0.9091
0281	0.0029	1 Myr	0.0293	203 Myr	0.9677
0781	0.0003	2 Myr	0.0096	203 Myr	0.9901
0870	0.0029	7 Myr	0.0293	102 Myr	0.9677
0951	0.0010	1 Myr	0.0312	203 Myr	0.9677
0953	0.0010	7 Myr	0.0312	509 Myr	0.9677
1078	0.0029	1 Myr	0.0880	509 Myr	0.9091
1488	0.0010	7 Myr	0.0312	203 Myr	0.9677
1684	0.0000	-	0.0909	203 Myr	0.9091
Additional sample					
0024	0.0029	1 Myr	0.0293	102 Myr	0.9677
0135	0.0010	3 Myr	0.0312	102 Myr	0.9677
0340	0.0074	1 Myr	0.0025	509 Myr	0.9901
1175	0.0050	1 Myr	0.0050	509 Myr	0.9901
1273	0.0025	2 Myr	0.0074	203 Myr	0.9901
1437	0.0161	8 Myr	0.0161	50 Myr	0.9677
1499	0.0081	9 Myr	0.2419	509 Myr	0.7500

Note. — M_y and age_y give the mass fraction and age of the young population, respectively. M_i and age_i are the same parameters for the intermediate-age population. The age of the old population was fixed at 5 Gyr; M_o gives its resulting mass fraction.

TABLE 5
Best fitting parameters using the "Starburst" library.

VCC	M_y	age_y	M_i	age_i	M_o
Main sample					
0021	0.0083	8 Myr	0.0826	500 Myr	0.9091
0281	0.0029	1 Myr	0.0293	200 Myr	0.9677
0781	0.0003	8 Myr	0.0096	100 Myr	0.9901
0870	0.0227	8 Myr	0.2273	500 Myr	0.7500
0951	0.0029	9 Myr	0.0880	500 Myr	0.9091
0953	0.0025	8 Myr	0.0074	100 Myr	0.9901
1078	0.0083	8 Myr	0.0826	200 Myr	0.9091
1488	0.0029	8 Myr	0.0880	500 Myr	0.9091
1684	0.0029	1 Myr	0.0880	500 Myr	0.9091
Additional sample					
0024	0.0029	5 Myr	0.0293	500 Myr	0.9677
0135	0.0025	5 Myr	0.0074	100 Myr	0.9901
0340	0.0050	1 Myr	0.0050	20 Myr	0.9901
1175	0.0050	1 Myr	0.0050	500 Myr	0.9901
1273	0.0025	2 Myr	0.0074	200 Myr	0.9901
1437	0.0083	1 Myr	0.0826	500 Myr	0.9091
1499	0.0081	8 Myr	0.2419	200 Myr	0.7500

Note. — Same as Table 4, but for the "Starburst" library.

TABLE 6
Best fitting parameters using the "BC03" library.

VCC	M_y	age_y	M_i	age_i	M_o
Main sample					
0021	0.0029	9 Myr	0.0880	509 Myr	0.9091
0281	0.0029	1 Myr	0.0880	509 Myr	0.9091
0781	0.0003	1 Myr	0.0096	203 Myr	0.9901
0870	0.0029	6 Myr	0.0293	203 Myr	0.9677
0951	0.0010	6 Myr	0.0312	203 Myr	0.9677
0953	0.0010	7 Myr	0.0312	509 Myr	0.9677
1078	0.0029	1 Myr	0.0880	509 Myr	0.9091
1488	0.0010	7 Myr	0.0312	203 Myr	0.9677
1684	0.0029	6 Myr	0.0880	509 Myr	0.9091
Additional sample					
0024	0.0029	5 Myr	0.0880	509 Myr	0.9091
0135	0.0010	4 Myr	0.0312	102 Myr	0.9677
0340	0.0029	1 Myr	0.0293	50 Myr	0.9677
1175	0.0029	1 Myr	0.0880	509 Myr	0.9091
1273	0.0025	2 Myr	0.0074	509 Myr	0.9901
1437	0.0029	3 Myr	0.0880	203 Myr	0.9091
1499	0.0081	8 Myr	0.2419	509 Myr	0.7500

Note. — Same as Table 4, but for the "BC03" library.

TABLE 7
HI detections.

VCC	$log(M_{\rm HI}/M_\odot)$	$\frac{M_{\rm HI}}{M_{\rm bary}}(\frac{M}{L}=3)$	$\frac{M_{\rm HI}}{M_{\rm bary}}(\frac{M}{L}=4.5)$	$\frac{M_{\rm HI}}{M_{\rm bary}}(\frac{M}{L}=6)$	Reference
Main sample					
0021	<7.78	<0.048	<0.032	<0.024	1
0170	7.39	0.014	0.009	0.007	2
0281	7.52	0.055	0.037	0.028	2
	7.74				3
0308	<7.92	<0.094	<0.065	<0.049	1
0781	<7.42	<0.055	<0.038	<0.028	1
0951	<6.84	<0.003	<0.002	<0.001	1
0953	<6.54	<0.009	<0.006	<0.004	1
1488	<8.27	<0.134	<0.093	<0.072	1
1779	<7.72	<0.041	<0.027	<0.021	1
1912	<7.44	<0.031	<0.021	<0.016	1
Additional sample					
0024	8.90	0.546	0.445	0.376	2
0135	<7.13	<0.009	<0.006	<0.004	2
	≤7.74				3
0334	7.89	0.339	0.255	0.204	2
0340	8.76	0.547	0.446	0.377	2
0446	7.62	0.284	0.209	0.166	2
0841	7.55	0.270	0.198	0.156	2
0890	7.27	0.106	0.073	0.056	2
1273	<7.10	<0.064	<0.044	<0.033	2
	≤7.54				3
1437	8.17	0.311	0.232	0.184	2
1499	<8.53	<0.256	<0.186	<0.147	4
1955	7.66	0.047	0.032	0.024	2
2007	7.31	0.218	0.157	0.122	2
	7.44				3
2033	7.39	0.045	0.031	0.023	2

Note. — HI masses and upper limits are given for our adopted Virgo cluster distance of $d = 15.85$Mpc. In columns 3 to 5 we list the ratios of the gas mass to the total baryonic mass, using different mass-to-light ratios as given in the column header; for details see text. References for the HI detections: 1. GOLDMine database (Gavazzi et al. 2003, http://goldmine.mib.infn.it/); 2. Gavazzi et al. (2005); 3. Huchtmeier & Richter (1989); 4. Huchtmeier & Richter (1986).

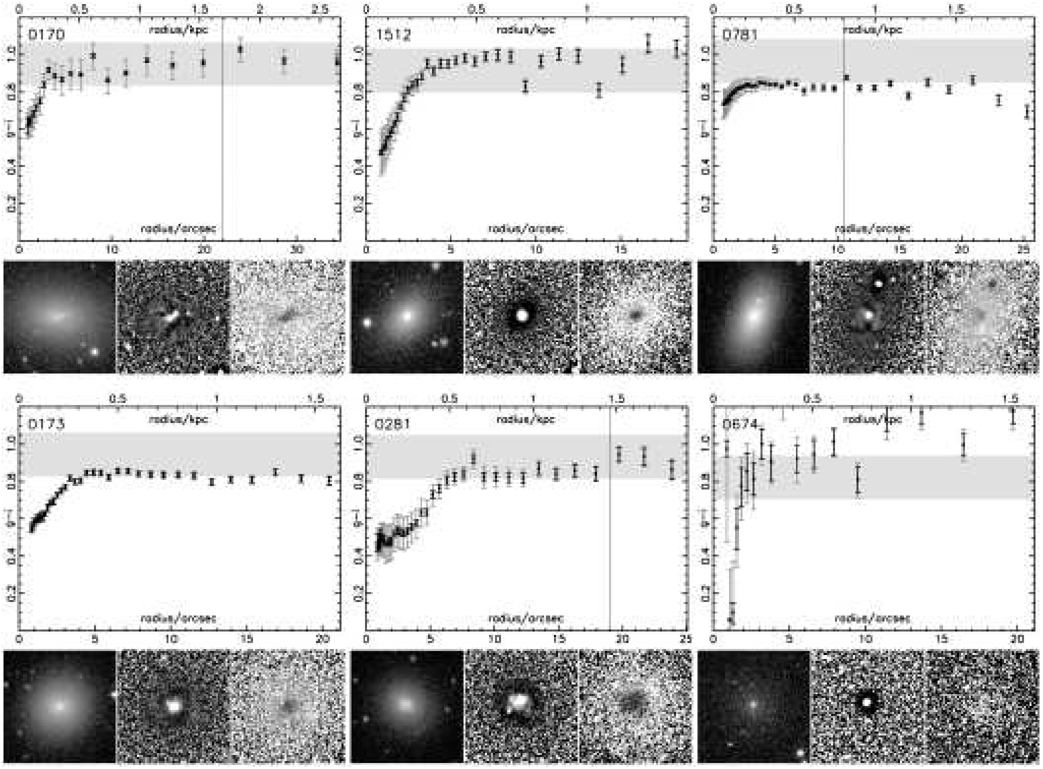

FIG. 1.— Early-type dwarfs with blue centers. For each galaxy, the radial $g-i$ color profile is shown (top panel; radius= $\sqrt{ab}$), along with the combined image (bottom left), the unsharp mask created with a Gaussian filter with $\sigma = 4$ pixels (bottom center), and the $g-i$ color map (bottom right). The combined images have a horizontal scale of $70''$, or 5.4 kpc with $d = 15.85$ Mpc, while the scales of unsharp masks and color maps are only half as large. A legend showing the grey scales of the color maps is given in Fig. 3. The galaxies are sorted such that those with a relatively constant outer color and an abruptly starting, steep gradient come first, while those with a gradual color change come last (in Fig. 3). The sorting has been done visually, without any quantitative basis. The black error bars in the color profiles give the uncertainty calculated from the S/N only, whereas the grey error bars represent the *azimuthal* variation of the color at the respective radius. Since the latter includes S/N-effects, the grey error bars are always larger than the black ones. The vertical dotted line denotes the half-light radius – if available – as given by Binggeli & Cameron (1993). The profiles are shown up to the estimated radius from Binggeli et al. (1985), at $\mu_{\rm B} \approx 25.5 {\rm mag/arcsec}^2$. The grey-shaded areas enclose the 2-σ-range of the colors of "ordinary" dEs (i.e. without a blue center) at the respective magnitude, as derived from Lisker et al. (2005). See text for details. For VCC 0674, the steps between each point are twice as large as for the other galaxies, due to its low S/N.

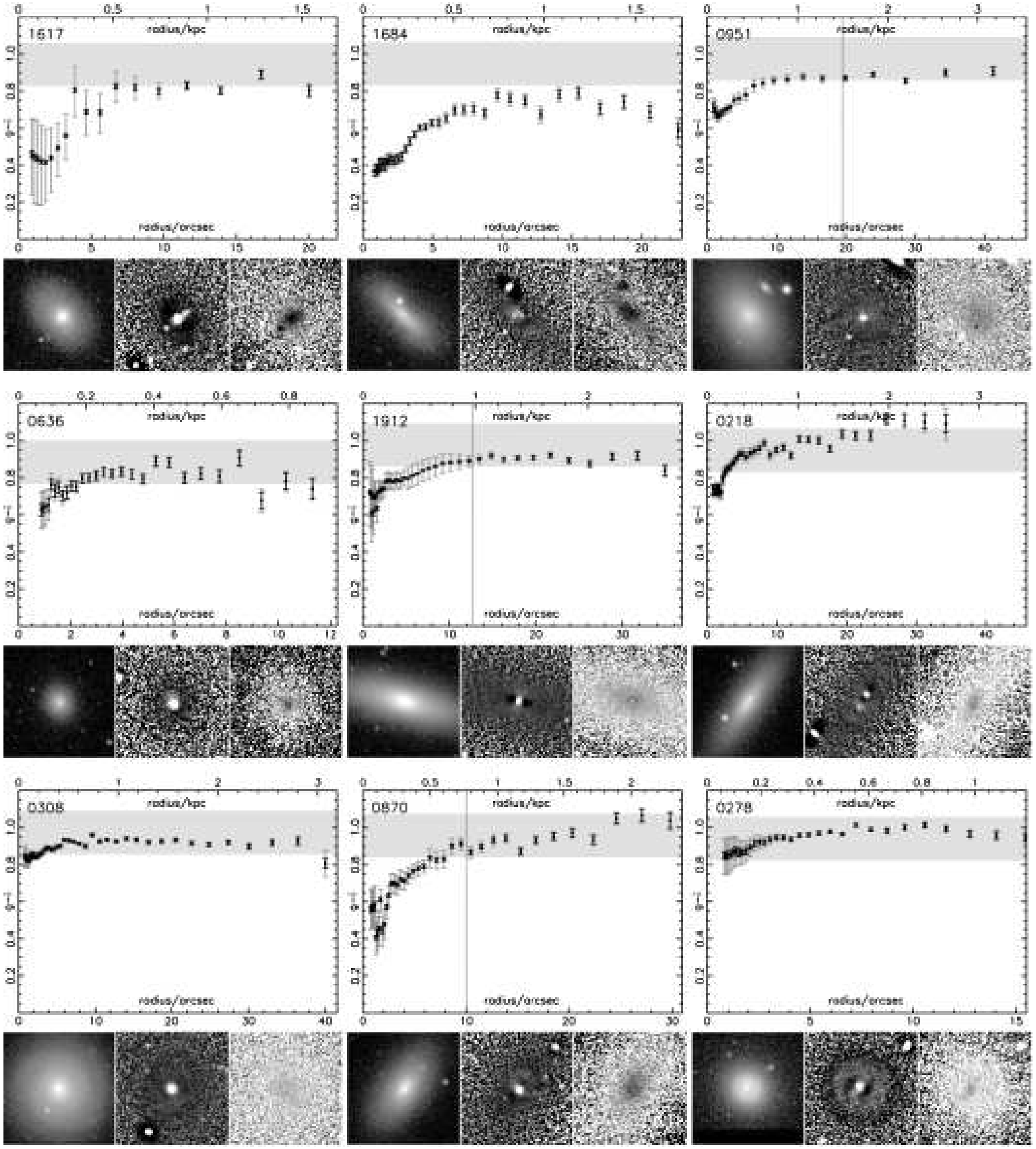

FIG. 2.— Early-type dwarfs with blue centers. Continued from Fig. 1.

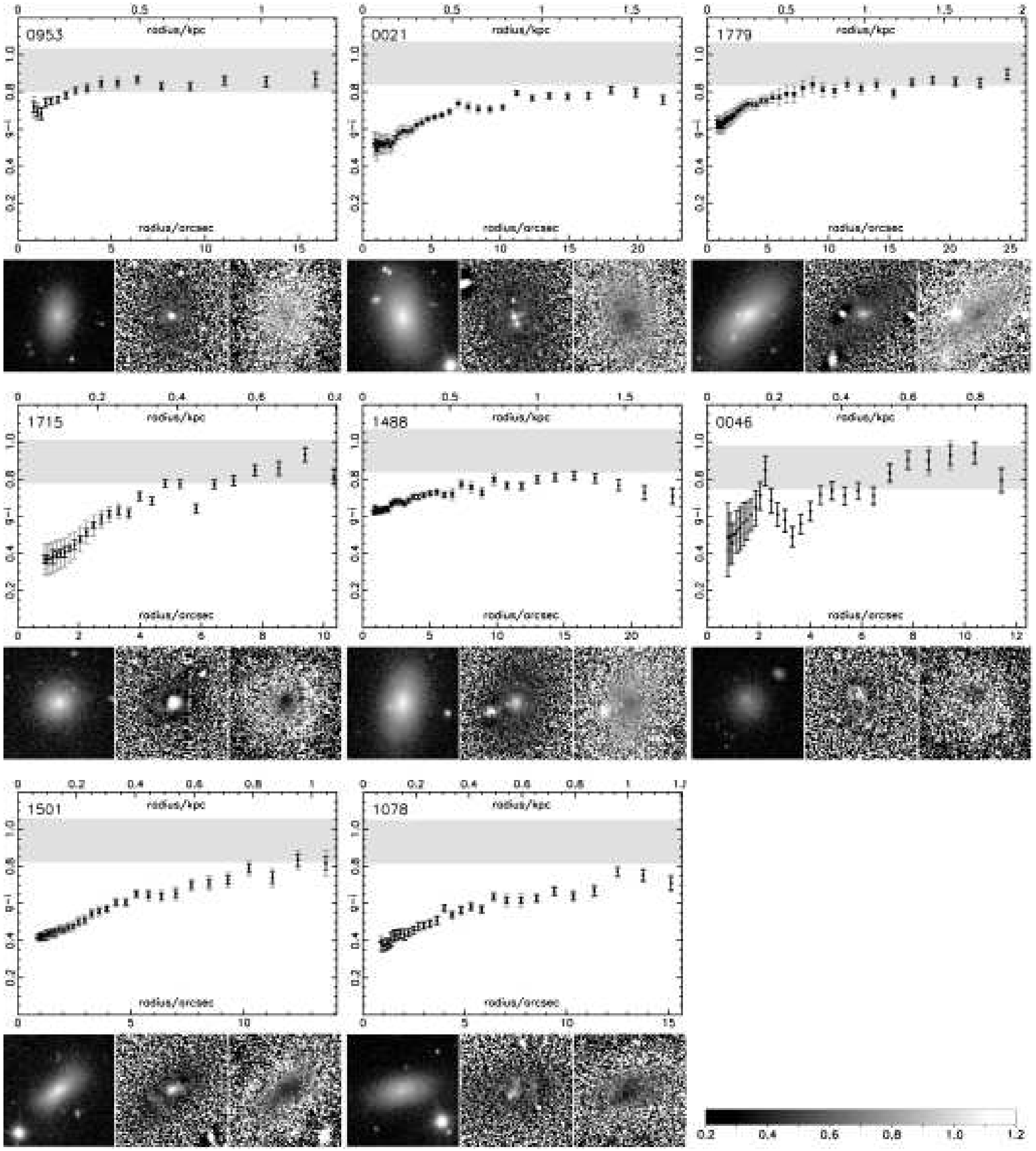

FIG. 3.— Early-type dwarfs with blue centers. Continued from Fig. 2. The bar in the bottom right panel indicates the grey scale used for the color maps.

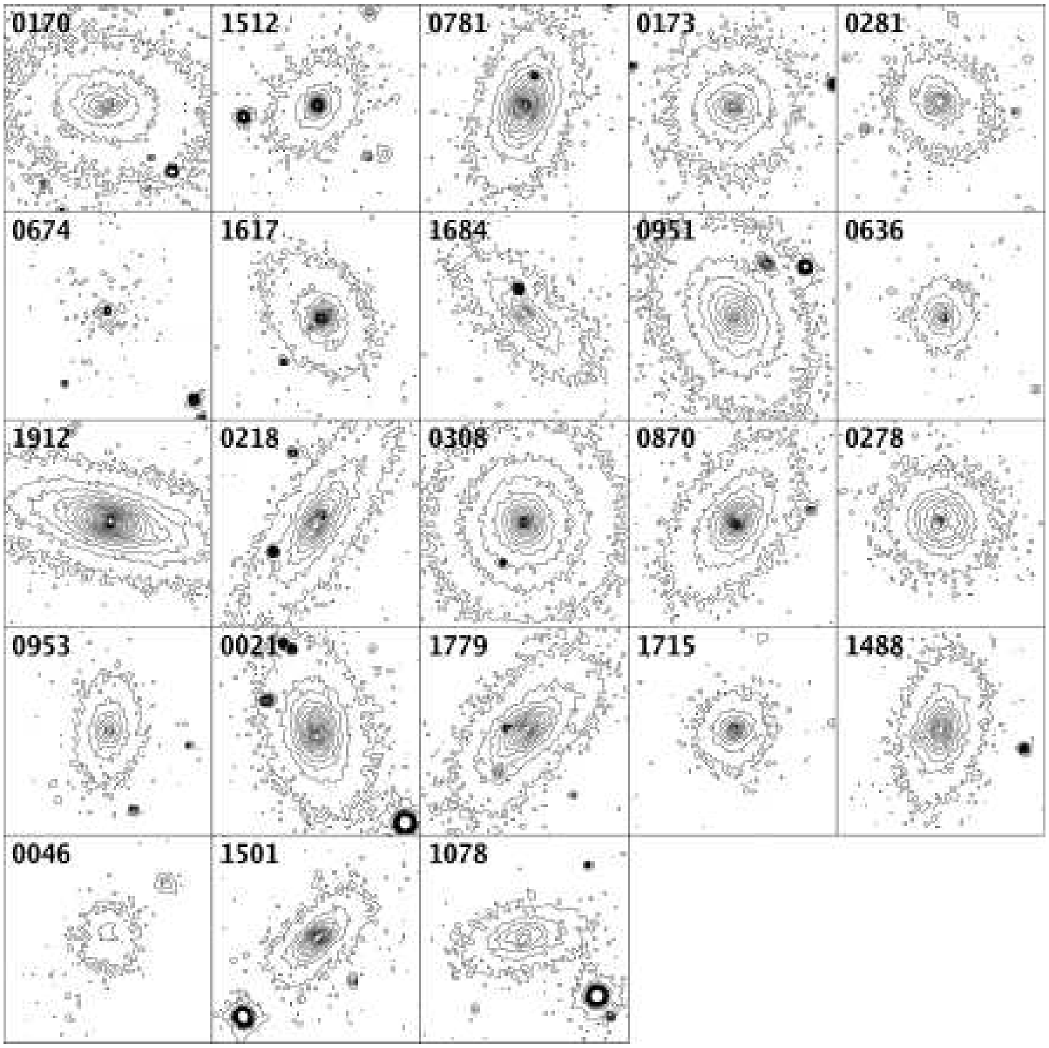

FIG. 4.— Isophotal contours of the dE(bc)s. The galaxies are shown in the same order as in Figs. 1 to 3. Contour diagrams were produced with *IRAF/newcont* on the combined images. The outermost contour lies at a level of three times the noise RMS, which was measured for each image separately. Contours are then displayed for 15 logarithmic steps up to 300 times the RMS.

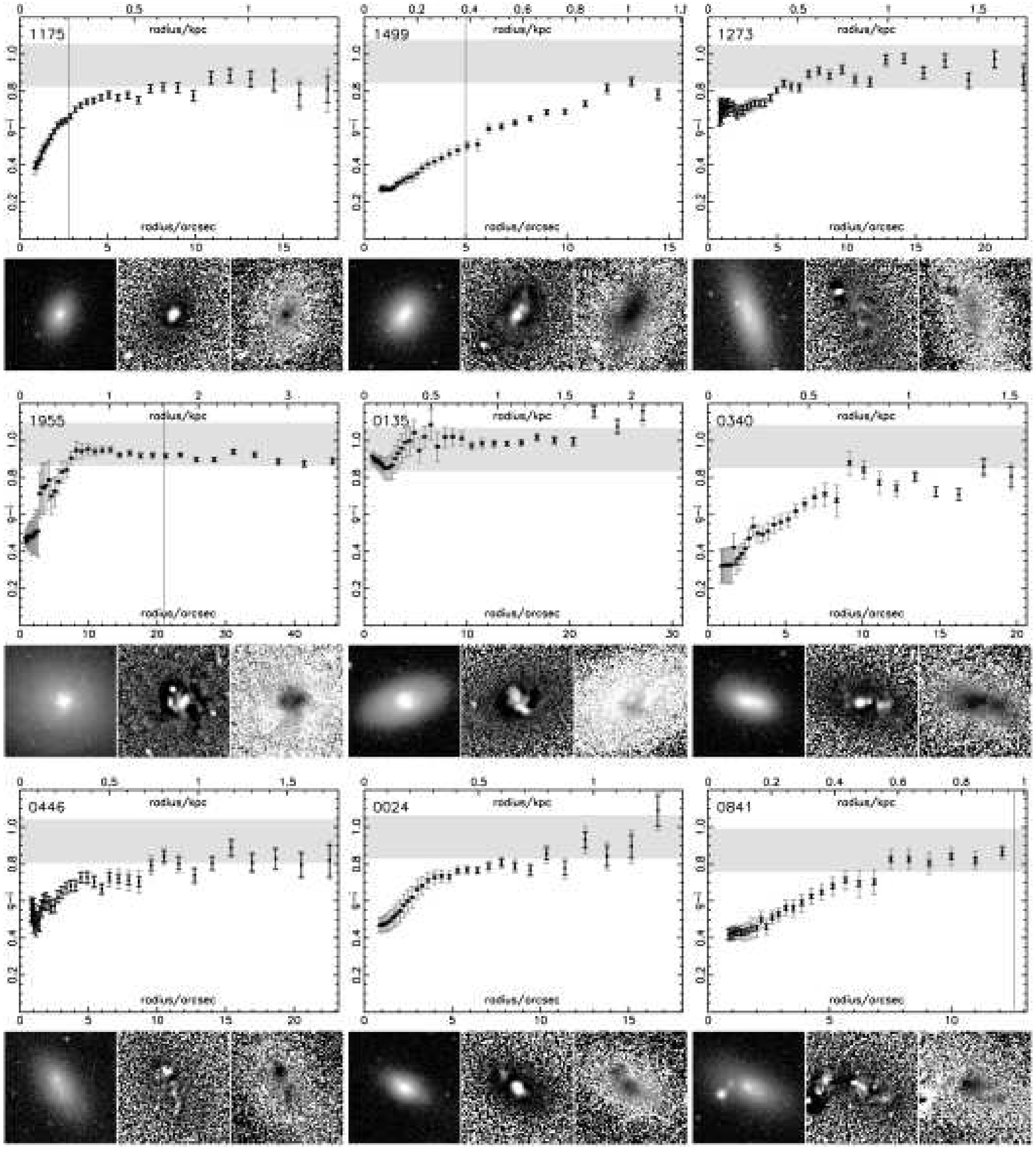

FIG. 5.— Galaxies similar to the dE(bc)s. Like Fig. 1, but for the galaxies of the additional sample, which were not classified as dEs but were chosen by us as being similar. The two top left galaxies were classified as E or S0; the top right galaxy as irregular. All other objects here and in Fig. 6 were classified as (candidate) BCDs, and are sorted according to the shape of the color gradient, analogous to Figs. 1 to 3.

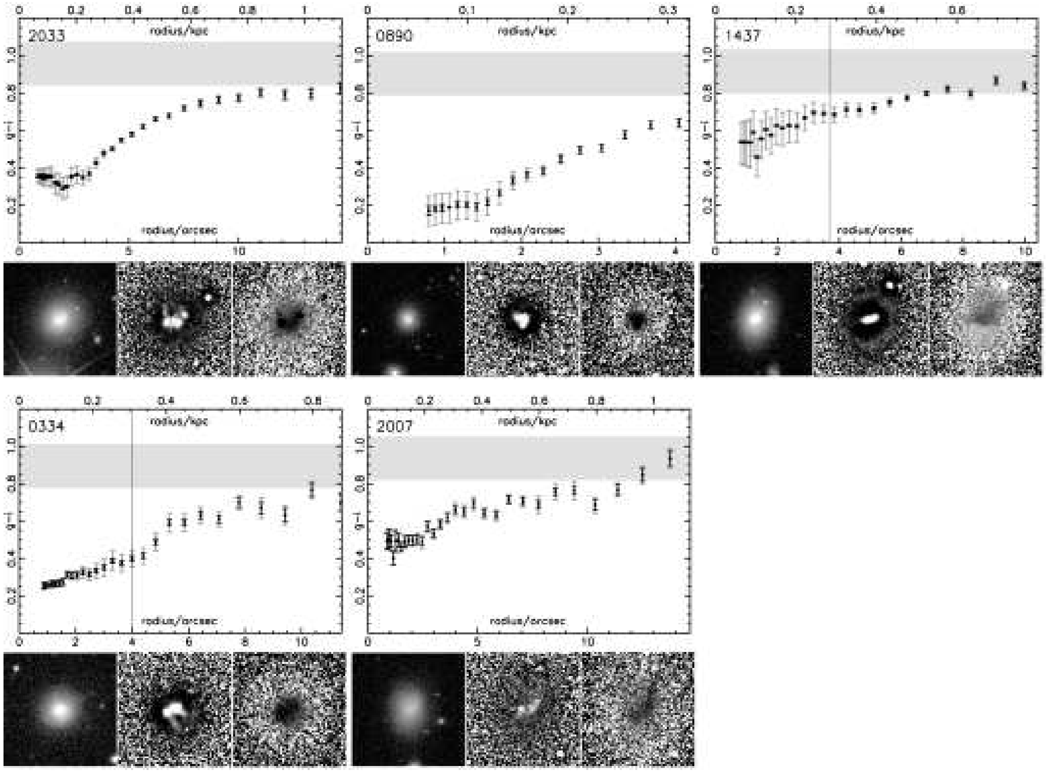

FIG. 6.— Galaxies similar to the dE(bc)s. Continued from Fig. 5.

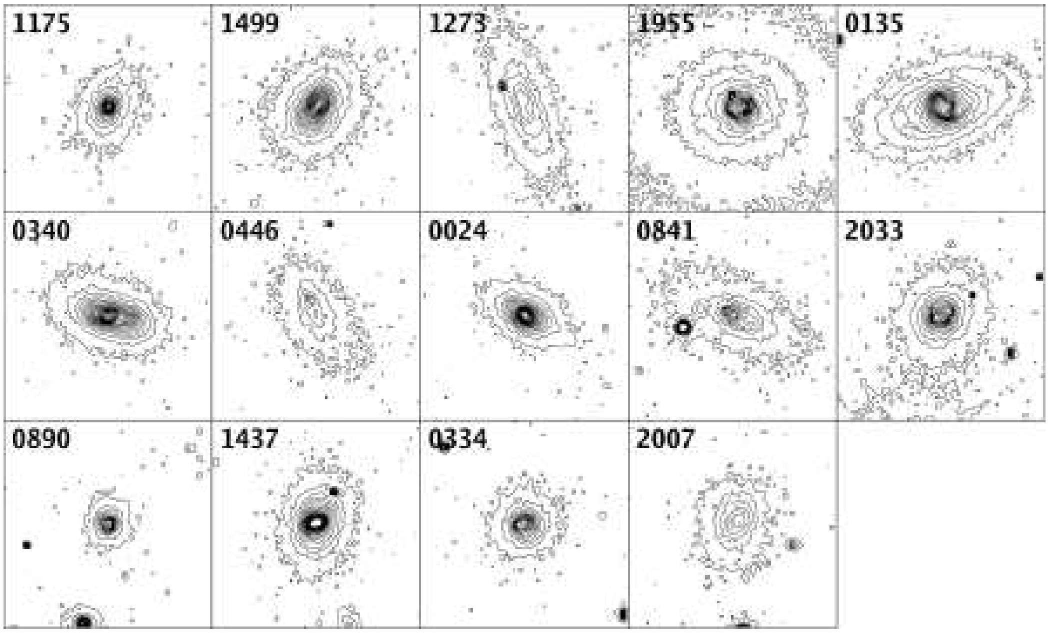

FIG. 7.— Isophotal contours of the additional sample. Like Fig. 4, but for the galaxies of the additional sample, which are shown in the same order as in Figs. 5 and 6.

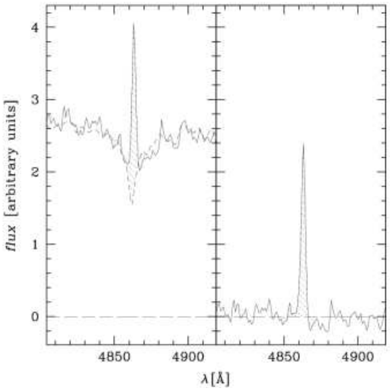

FIG. 8.— Emission line strength. Illustration of how the Hβ emission line strength was measured for the example of VCC 0870. In the left panel, the solid line represents the observed spectrum, whereas the short-dashed line shows the best fit using the "BC03" SSP library. The shaded region between these two lines shows the area used to calculate the emission line strength. The right panel shows the emission line after subtracting the (rebinned) best fit. The shaded area corresponds to the shaded area between spectrum and best fit from the left panel.

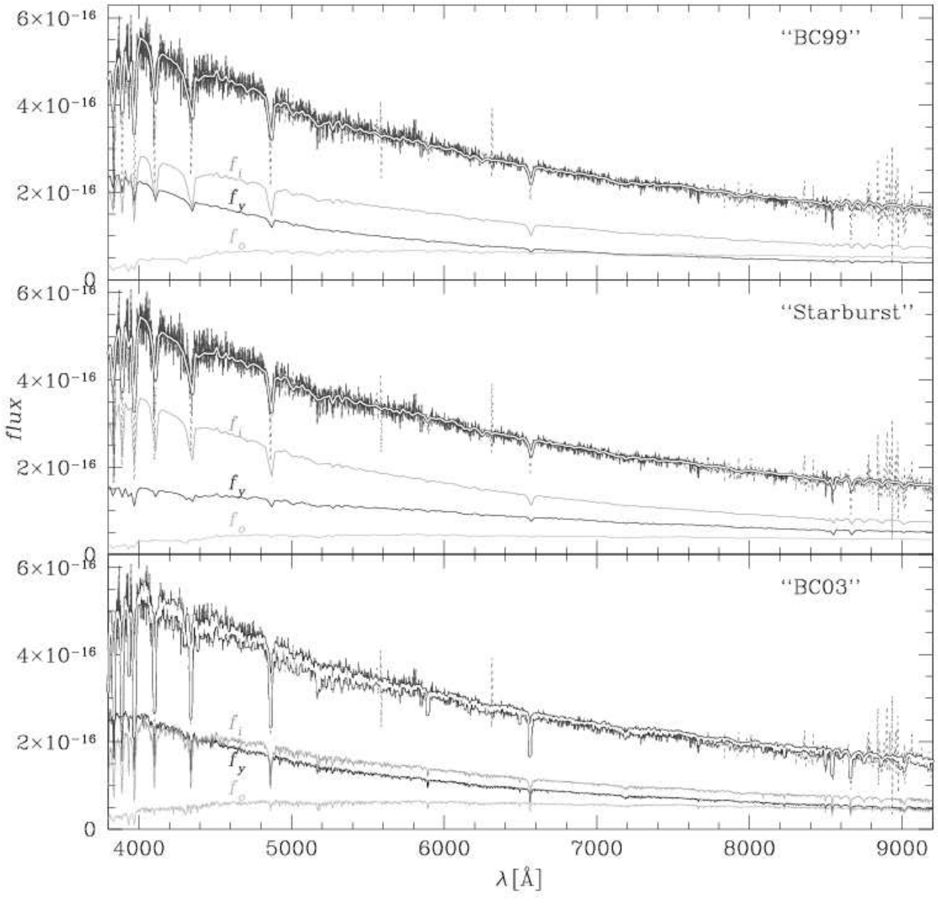

FIG. 9.— Example of a "best fit". The thin (red or dark grey) lines represent the observed spectrum (VCC 1499), the thicker white lines show the best fitting spectra obtained using the different SSP libraries, whereas the lower-level lines show the best fits decomposed into the young (f_y, blue or dark grey), the intermediate-age (f_i, green or medium grey), and the old (f_o, cyan or light grey) populations. Flux is given in erg cm^{-2} s^{-1} Å^{-1}.

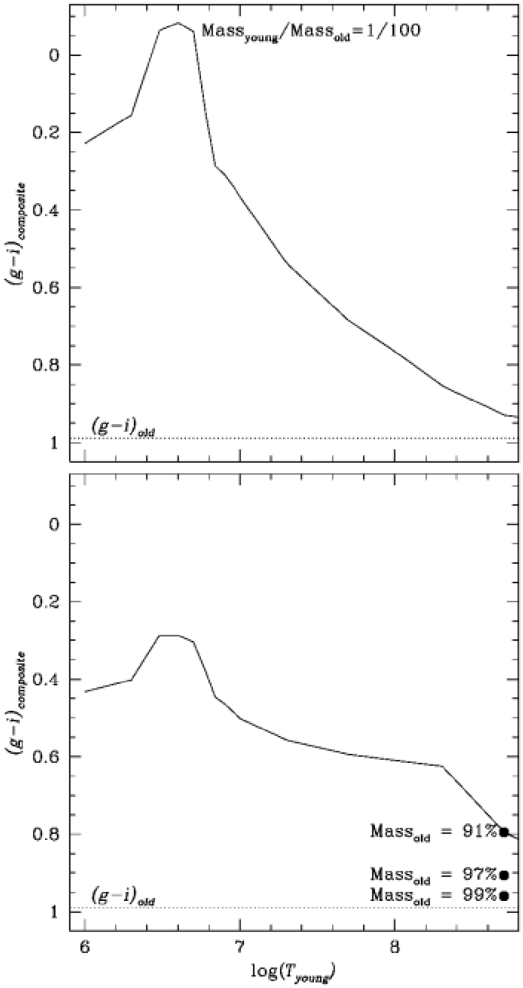

FIG. 10.— Color evolution of an ageing population. Evolution of $g-i$ color of different composite stellar populations. The age of the old population is fixed at 5 Gyr, and the metallicity of all populations is fixed at [Fe/H] = −0.3. *Upper panel:* Composite population made out of a young and an old population. The young population makes up for 1% of the total mass. *Lower panel:* Composite population made out of a young, an intermediate-age, and an old population, similar to the best fit results derived for the dE(bc)s. The upper curve represents a population with $(M_y + M_i){:}M_o = 1{:}10$, $M_y{:}M_i = 1{:}30$, with $M_{y,i,o}$ denoting the mass fractions of young, intermediate-age, and old population, respectively. The intermediate-age population is chosen to be ∼500 Myr older than the young one. The big black dots mark the color of this mixture after 500 Myr, as well as that of two other mixtures: $\{(M_y + M_i){:}M_o = 1{:}30$, $M_y{:}M_i = 1{:}30\}$ (middle dot), and $\{(M_y + M_i){:}M_o = 1{:}100$, $M_y{:}M_i = 1{:}10\}$ (lower dot).

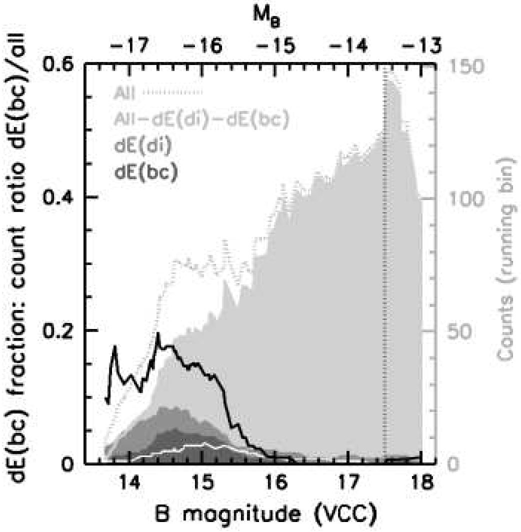

Fig. 11.— Luminosity function. Running histogram of the number of galaxies (right y-axis) with respect to B-band magnitude as given by the VCC. Shown are dE(bc)s of the main sample (dark grey area), dE(di)s (medium grey area), all dEs excluding both dE(di)s and dE(bc)s (light grey area), and all dEs (light grey dashed line). Galaxies of the additional sample – which by construction are not included in the dE sample – are represented by the white line. The bin-width is $1\overset{\mathrm{m}}{.}0$, therefore the counts are incomplete for $m_{\mathrm{B}} > 17\overset{\mathrm{m}}{.}5$ (vertical dotted line). A bin is calculated at each position of a galaxy in the full sample. Only galaxies with certain cluster membership are taken into account. The fraction of dE(bc)s – the ratio of the dE(bc) histogram to the histogram of all dEs – is given as black line (left y-axis applies). The upper x-axis gives absolute magnitudes assuming $m - M = 31\overset{\mathrm{m}}{.}0$.

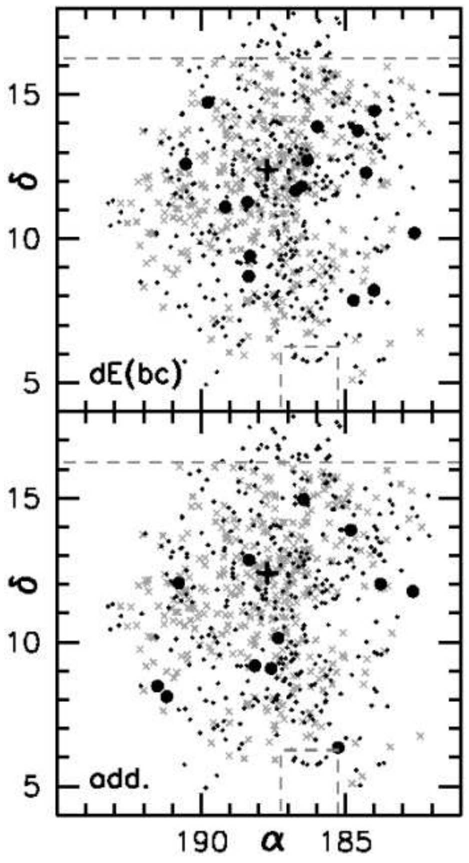

Fig. 12.— Distribution within the cluster. Projected spatial distribution of the dE(bc)s of the main sample (black circles, upper panel) and the galaxies of the additional sample (black circles, lower panel). Coordinates are given for J2000. Grey crosses represent all dEs without blue centers. All other Virgo cluster galaxies with $m_{\mathrm{B}} \leq 18\overset{\mathrm{m}}{.}0$ are shown as small black dots. Only galaxies with certain cluster membership are considered. The black cross gives the position of M87. Boundaries of the SDSS coverage are shown as grey dashed lines.

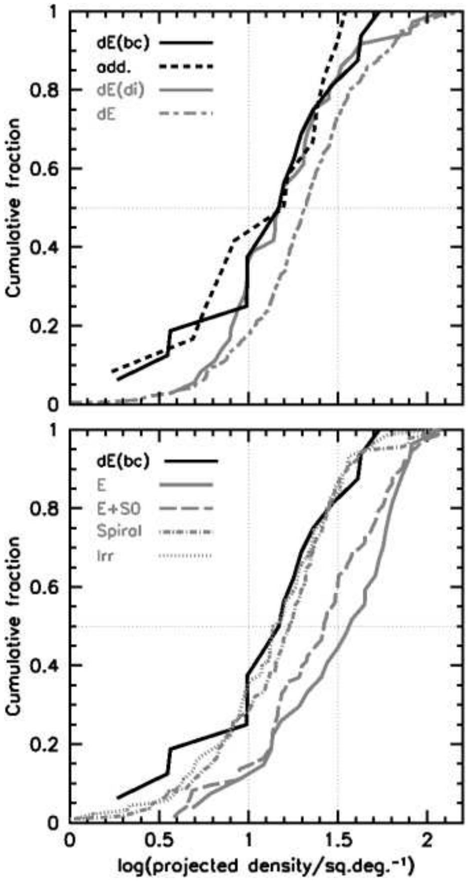

Fig. 13.— Morphology vs. density. Cumulative distribution of local projected densities. Following Dressler (1980) and Binggeli et al. (1987), we define a circular area around each VCC galaxy that includes its ten nearest neighbours (independent of galaxy type), yielding a projected density (number of galaxies per square degree). Only galaxies with certain cluster membership are taken into account. *Upper panel:* The dE(bc)s of the main sample (solid black line), the galaxies of the additional sample (dashed black line), the dE(di)s from Paper I (solid grey line), and ordinary dEs (excluding dE(bc)s and dE(di)s, dashed grey line). *Lower panel:* The dE(bc)s of the main sample (solid black line) compared to various Hubble types.

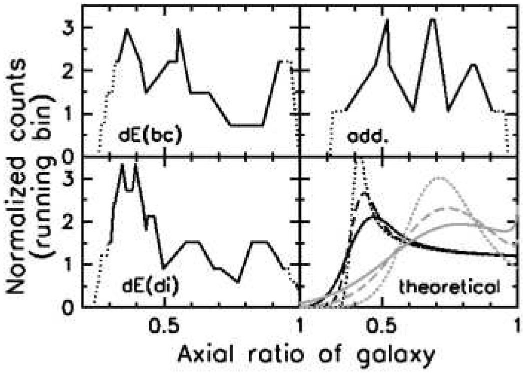

Fig. 14.— Flattening distribution. Distribution of projected axial ratios of the dE(bc)s of the main sample (top left), the galaxies of the additional sample (top right), and the dE(di)s from Paper I (bottom left). The data are shown as running histogram with a bin-width of 0.1. Only galaxies with certain cluster membership are considered. Beyond the last data point on each side, the histograms are plotted with dotted instead of solid lines. The bottom right hand panel shows theoretically expected curves for intrinsic oblate (black) and prolate (grey) shapes, assuming randomly distributed inclinations and intrinsic axial ratios that are described by the following Gaussian distributions: oblate with mean $\mu = 0.4$ and $\sigma = 0.07$ (black solid line), $\sigma = 0.04$ (black dashed line), $\sigma = 0.02$ (black dotted line); prolate with $\mu = 0.65$ and $\sigma = 0.2$ (grey solid line), $\sigma = 0.15$ (grey dashed line), $\sigma = 0.1$ (grey dotted line).

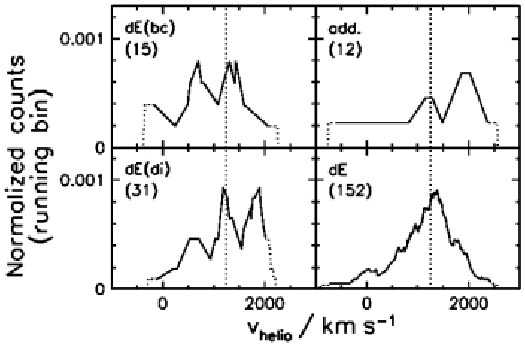

FIG. 15.— Velocity distribution. Distribution of available heliocentric velocities, taken from the NASA/IPAC Extragalactic Database (NED). The dE(bc)s of the main sample are shown in the top left panel, the galaxies of the additional sample in the top right panel, the dE(di)s from Paper I in the bottom left panel, and the remaining dEs (excluding dE(bc)s and dE(di)s) in the bottom right panel. Only galaxies with certain cluster membership are included. The vertical dotted line marks the value of $v_{\rm helio}$ = 1248 km s^{-1}, which is the median value of all 194 available velocities for early-type dwarfs. The data are shown as running histogram with a bin-width of 366km s^{-1}, corresponding to the semi-interquartile range of these 194 velocities. Numbers in brackets are the number of galaxies included in the respective panel. Beyond the last data point on each side, the histograms are plotted with dotted instead of solid lines